

1 **Methylo trophic methanogenesis in the Archaeoglobi: Cultivation of *Ca.*** 2 ***Methanoglobus hypatiae* from a Yellowstone hot spring**

3
4 Mackenzie M. Lynes¹, Zackary J. Jay¹, Anthony J. Kohtz¹, Roland Hatzenpichler^{1,2,*}

5
6 ¹ Department of Chemistry and Biochemistry, Center for Biofilm Engineering, and Thermal Biology
7 Institute, Montana State University, Bozeman, MT 59717, USA

8 ² Department of Microbiology and Cell Biology, Montana State University, Bozeman, MT 59717, USA

9 * Corresponding author: Roland Hatzenpichler, email: roland.hatzenpichler@montana.edu

10
11 **ORCID Numbers of Authors:** M.M.L., 0000-0002-9410-0285; Z.J.J., 0000-0003-3062-4933; A.J.K.,
12 0000-0002-0561-8710; R.H., 0000-0002-5489-3444

13 **Competing Interest Statement:** none declared.

14 **Abstract**

15
16 Over the past decade, environmental metagenomics and PCR-based marker gene surveys have
17 revealed that several lineages beyond just a few well-established groups within the Euryarchaeota
18 superphylum harbor the genetic potential for methanogenesis. One of these groups are the Archaeoglobi, a
19 class of obligately thermophilic Euryarchaeotes that have long been considered to live a non-methanogenic
20 lifestyle. Here, we enriched *Candidatus* *Methanoglobus hypatiae*, a methanogen affiliated with the family
21 Archaeoglobaceae, from a hot spring in Yellowstone National Park. The enrichment is sediment-free, grows
22 at 64-70 °C and a pH of 7.8, and produces methane from mono-, di-, and tri-methylamine. *Ca. M. hypatiae*
23 is represented by a 1.62 Mb metagenome-assembled genome with an estimated completeness of 100% and
24 accounts for up to 67% of cells in the culture according to fluorescence *in situ* hybridization. Via genome-
25 resolved metatranscriptomics and stable isotope tracing, we demonstrate that *Ca. M. hypatiae* expresses
26 methylo trophic methanogenesis and energy-conserving pathways for reducing monomethylamine to
27 methane. The detection of Archaeoglobi populations related to *Ca. M. hypatiae* in 36 geochemically diverse
28 geothermal sites within Yellowstone National Park (pH 2.61-9.35; 18.4 to 93.8 °C), as revealed through the
29 examination of previously published gene amplicon datasets, implies a previously underestimated
30 contribution to anaerobic carbon cycling in extreme ecosystems.

31 **Significance statement**

32
33 The majority of global methane emissions are attributed to the activity of methane-producing
34 anaerobic archaea, the methanogens. Over the last decade, environmental DNA sequencing demonstrated
35 that culture collections do not adequately represent the true taxonomic and metabolic diversity of
36 methanogens present in nature. One group of archaea postulated to contribute to methane production in
37 high temperature marine and terrestrial environments are the Archaeoglobi, a group of obligate
38 thermophilic archaea within the Euryarchaeota superphylum. Here, we report the cultivation and
39 physiological characterization of a methanogenic member of the Archaeoglobi, *Ca. Methanoglobus*
40 *hypatiae*, from a hot spring in Yellowstone National Park. Via a combination of growth experiments, stable
41 isotope tracing, metatranscriptomics, microscopy analyses, and re-examination of gene amplicon surveys,
42 our study provides direct experimental evidence of methanogenesis in the Archaeoglobi and shows that
43 closely related archaea are widely distributed in Yellowstone's geothermal features.

44 **Introduction**

45 Methanogenesis is one of the most ancient metabolic pathways and plays a major role in the
46 biogeochemical carbon cycle. Phylogenomic reconstructions and geological evidence suggest that
47 methanogenesis was among the earliest metabolisms to evolve and that the last common ancestor of all
48 extant archaea likely was a methanogen (1-9). Therefore, the study of methanogens is essential for
49 understanding the co-evolution of life and the biosphere. Methanogenic archaea are the primary producers
50 of biogenic methane (CH₄) and contribute approximately 60% to the estimated 576 Tg of annual global
51 methane emissions to the atmosphere (10, 11). Methanogenic pathways are classified based on the specific
52 substrate that is reduced to produce methane (12-14). All methanogenic pathways converge at the terminal
53 methane-forming step catalyzed by the methyl-coenzyme M reductase (MCR) complex. MCR and its
54 homologs also catalyze the reversible reaction in the anaerobic oxidation of alkanes in alkanotrophic
55 archaea (15, 16). MCR is uniquely present in all methanogens and is commonly used to identify potential
56 methane and/or alkane cycling archaea in sequencing surveys (12, 17).

57 The physiology and biochemistry of methanogens has near-exclusively been investigated in axenic
58 cultures of microorganisms belonging to the Euryarchaeota superphylum (12, 17-19). These predominantly
59 grow by acetoclastic or CO₂-reducing hydrogenotrophic methanogenesis, with limited observations of
60 Euryarchaeota exclusively using methylated precursors (12, 20, 21). As a result, methylotrophic
61 methanogenesis was considered to be of very limited environmental distribution. The extensive use of
62 environmental metagenomics has led to the discovery of metagenome-assembled genomes (MAGs)
63 encoding MCR from new lineages that are prevalent in anoxic environments, both within and outside the
64 Euryarchaeota (2, 12, 22-26).

65 The majority of MAGs affiliated with archaeal phyla outside the Euryarchaeota are predicted to be
66 methyl-reducing methanogens, with the exception of *Candidatus* (*Ca.*) Nezaarchaeota (25, 27) and *Ca.*
67 Methanomixophus affiliated with the order Archaeoglobales, which have been hypothesized to be CO₂-
68 reducing hydrogenotrophic methanogens (12, 25, 28). This result is consistent with the observation that
69 methylated methanogenic substrates, including different methylamines and methanol, are prevalent in the
70 environment, although their concentrations in hot springs is currently unknown. Further, methyl-reducing
71 methanogenesis is considered the predominant mode of methanogenesis in anoxic marine, freshwater, and
72 hypersaline sediments (reviewed in (20)).

73 Members of the class Archaeoglobi have long been considered non-methanogenic with isolates
74 characterized as dissimilatory sulfate reducers brought into culture as early as 1987 (29). To date, only nine
75 species of the class Archaeoglobi have been obtained in axenic culture, and all were sourced from marine
76 hydrothermal systems or off-shore oil reservoirs (30). The discovery of both MCR (25, 31, 32) and methyl-
77 H₄M(S)PT:coenzyme M methyltransferase (MTR) complexes in genomes of the Archaeoglobaceae have
78 suggested that members of this family may live by methanogenesis rather than by sulfate reduction (28).

79 Very recently, important progress towards experimental verification of methanogenesis by members
80 of this family has been made. Liu *et al.* reported the *in situ* expression of genes related to hydrogen-
81 dependent methylotrophic methanogenesis and heterotrophic fermentation within populations of
82 Archaeoglobi in a high-temperature oil reservoir (28). Lynes, Krukenberg *et al.* reported that Archaeoglobi
83 can be enriched in hot spring mesocosms under methanogenic conditions (33). Wang *et al.* reported that
84 *mcrABG* and other methanogenesis marker genes encoded by two Archaeoglobales MAGs were highly
85 expressed in hot spring microcosms incubated at 65 °C and 75 °C (34). Importantly, one of these
86 Archaeoglobales MAGs represented the only Mcr-encoding archaeon that expressed *mcrABG* genes in
87 methanogenic microcosms performed without substrate addition or with the addition of 10 mM methanol

88 at 75 °C. This indirectly demonstrated the methanogenic nature of this archaeon (34). Last, Buessecker *et*
89 *al.* reported the establishment of a methanogenic enrichment culture of *Ca. Methanoglobus nevadensis* from
90 Great Boiling Spring (NV, USA) (35). The culture yields up to 158 μmol of methane per liter after two
91 weeks of incubation at its optimal growth temperature of 75 °C. *Ca. M. nevadensis* is represented by a 63%
92 complete MAG obtained from the culture (35).

93 Here, we report on the enrichment cultivation of *Ca. Methanoglobus hypatiae* LCB24, a methanogen
94 affiliated with the family Archaeoglobaceae, from a hot spring in Yellowstone National Park (YNP). Using
95 a combination of targeted cultivation, growth experiments, microscopy, stable isotope tracing,
96 metagenomics, and metatranscriptomics, we demonstrate that *Ca. M. hypatiae* lives by methylotrophic
97 methanogenesis and converts different methylamines to methane. By examining previously published
98 datasets for the presence of Mcr-encoding Archaeoglobi, we demonstrate that these archaea are distributed
99 in geothermal features of YNP, where they likely contribute to anaerobic carbon cycling. Our study
100 represents the first direct experimental evidence of a methanogen within the Archaeoglobaceae and adds to
101 the growing body of evidence demonstrating that methanogenesis is widely spread within the Euryarchaeota
102 superphylum.

103

104 **Results and Discussion**

105 **Cultivation**

106 In our recent survey on the diversity of Mcr-encoding archaea in the geothermal features of YNP,
107 mesocosms seeded with biomass from a hot spring located within the Lower Culex Basin (LCB024; pH 7-
108 8, 56-74 °C), had shown potential to enrich for methanogenic Archaeoglobi (33). Using a sediment slurry
109 collected from LCB024, we initiated incubations supplied with monomethylamine (MMA) and antibiotics
110 incubated in anoxic media (pH 7.8, 70 °C) under a N₂ headspace. The relative abundance, as determined by
111 16S rRNA gene amplicon sequencing, of Archaeoglobi-affiliated organisms in LCB024 was 0.32% in the
112 initial slurry and had fallen to 0.02% by the time incubations were initiated a few months after samples had
113 been collected (Fig. 1A).

114 Methane was detected after 36 days in the initial enrichment and the culture transferred to fresh media
115 after reaching the late exponential phase of methane production following 70 days of incubation (447 μM ;
116 Fig. 1B). Five Archaeoglobi related 16S rRNA gene amplicon ASVs were identified in the initial
117 enrichment, however one ASV grew to dominate the microbial community after the first transfer and
118 reached 74.8% relative abundance after 62 days. In the transfers that followed, Archaeoglobi-related
119 sequences became the only archaeal reads detected by 16S rRNA gene amplicon sequencing with the
120 second most abundant organism a bacterium affiliated with the *Pseudothermotoga* at 6.80%. While the
121 CO₂-reducing methanogen *Methanothermobacter* sp. was detected at 0.45% relative abundance in the
122 slurry material used for inoculation, it was not detected in any subsequent transfers, nor were any other
123 methanogens. Over subsequent transfers (238 days, T2-T5), the relative abundance of Archaeoglobi ASVs
124 ranged from 46 to 69% and the final methane yield steadily increased from 1,844 to 2,459 μM . A sediment-
125 free enrichment was obtained by the third transfer. Starting with the fourth transfer, the culture volume was
126 scaled from 30 mL to 50 mL and designated as culture LCB24. By the sixth transfer, the culture produced
127 3,943 μM methane within 34 days. Metagenomic sequencing at two timepoints (day 335 of the enrichment
128 and day 33 of the isotope tracing experiment described below) and 16S rRNA gene amplicon sequencing
129 over recurring transfers (Fig. 1A) demonstrated that ASVs and MAGs affiliated with Archaeoglobi
130 represented the only archaeon in culture LCB24. A single Mcr complex (*mcrAGCDB*) belonging to the

131 Archaeoglobi MAG was present, indicating this MAG exclusively represented the only population with
132 methanogenic potential.

133

134 **Metagenomics and Phylogenetics**

135 The reconstructed LCB24 MAG of the Mcr-encoding archaeon was 1.62 Mbp in length with an
136 estimated completeness of 100% according to checkM (SI Appendix, Table S3). This MAG was the result
137 of a combined assembly of the T4-MG and SIT-MG genomes as this method yielded an improved assembly.
138 Therefore, it was used for phylogenomic analysis against Archaeoglobi reference MAGs and genomes
139 using 33 conserved single copy marker proteins and 16S rRNA genes (Fig. 2AB, SI Appendix, Table S4).
140 Interestingly, MAGs that encoded Mcr complexes exhibited distinct clustering when assessed using a set
141 of marker proteins, setting them apart from those lacking *mcr* gene sequences. Consistently, 16S rRNA
142 gene phylogeny supported this clustering with a pronounced separation of reference genomes and MAGs
143 based on geographical origin, resulting in three main clusters: (i) those retrieved from North American hot
144 springs (YNP and Great Boiling Spring, GBS), (ii) those originating from hot springs in China, and (iii)
145 those obtained from deep-sea marine hydrothermal systems (Fig. 2B). The examination of conserved
146 marker proteins also revealed two distinct clades of Archaeoglobi within YNP features, categorized by the
147 presence or absence of Mcr complexes.

148 LCB24 and closely related reference MAGs and isolate genomes exhibited a range of amino acid
149 identities (AAI, 52.6-98.6%; Fig. 2C). Altogether, the LCB24 MAG was found to be highly related to
150 previously obtained Archaeoglobi MAGs encoding the MCR complex and only distantly related to
151 confirmed sulfate-reducing Archaeoglobales (AAI, 58.9-65%; ANI, 70.3-70.6%; 16S rRNA ANI, 91.6-
152 93.8%; SI Appendix Fig. S1, S2). Based on AAI, MAG LCB24 was most closely related to Archaeoglobi
153 LCB024-003 MAG (AAI, 98.6%), which we had obtained from the same hot spring in a previous study
154 (33). The ANI and AAI values to the closest cultured methanogen, *Ca. Methanoglobus nevadensis* GBS,
155 are 80.2 and 83.3%, respectively. Based on these results, we designate this archaeon *Ca. Methanoglobus*
156 *hypatiae* strain LCB24, named after the philosopher Hypatia of Alexandria (for a protologue, see the SI
157 Appendix, Results and Discussion). The estimated relative abundance of *Ca. M. hypatiae* based on the SIT-
158 MG was 92.8%. Other community members in the LCB24 culture with >1% relative sequence abundance
159 included members of the *Pseudothermotoga* (3.2%), *Desulfoviregula* (1.7%), and the family Moorellaceae
160 (1.3%) (Fig. 1A, Dataset S1).

161 The only *mcrAGCDB* genes recovered from both metagenomes belong to the genome of *Ca. M.*
162 *hypatiae*. Phylogenetic analysis of the single copy of McrA indicated its close relationship to McrA
163 sequences found in members of the TACK superphylum (Fig. 2D). This contrasts with the placement of
164 *Ca. M. hypatiae* within the Euryarchaeota based on phylogenomics (Fig. 2A), suggesting that Archaeoglobi
165 could have obtained the Mcr complex as a result of a horizontal gene transfer event from an archaeon in
166 the TACK superphylum (7, 8). Alternatively, it could indicate that non-methanogenic Archaeoglobi lost
167 the capacity for anaerobic methane cycling after they had diverged from a shared methanogenic ancestor.

168

169 **Methanogenic Activity of *Ca. M. hypatiae***

170 To gain insight into the activity of *Ca. M. hypatiae* under methanogenic and non-methanogenic
171 conditions, a stable isotope tracing (SIT) experiment was conducted. Cultures were incubated in the
172 presence of 10 mM of MMA; 8 mM of substrate were isotopically light, while the remaining 2 mM
173 consisted of either ¹³C-monomethylamine (¹³CH₃-NH₂) or D₃-monomethylamine (CD₃-NH₂). Addition of
174 the methanogenesis inhibitor bromoethanesulfonate (BES) was used as a non-methanogenic control (Fig.

175 1B, 3, SI Appendix, Fig. S3). On average across six replicates, the cultured converted $^{13}\text{CH}_3\text{-NH}_2$ to 356
176 $\mu\text{M } ^{13}\text{CH}_4$ (17.8%) and $138.71 \mu\text{M } ^{13}\text{CO}_2$ (6.9%) by day 32 (Fig. 3AC, Dataset S2). The conversion of $\text{CD}_3\text{-}$
177 NH_2 was nearly identical yielding $355 \mu\text{M } \text{CD}_3\text{H}$ (Fig. 3B). In the exponential phase of methane production,
178 five of the six replicates were harvested for metagenomic and metatranscriptomic sequencing while the
179 sixth replicate was allowed to grow to stationary phase. The replicate allowed to grow in each respective
180 experiment converted the provided $^{13}\text{CH}_3\text{-NH}_2$ to $717.7 \mu\text{M } ^{13}\text{CH}_4$ (35.9%) and $212.95 \mu\text{M } ^{13}\text{CO}_2$ (10.65%)
181 or $\text{CD}_3\text{-NH}_2$ to $394.76 \mu\text{M } \text{CD}_3\text{H}$ (19.7%) by day 38 (Fig. 3ABC). These results confirmed
182 monomethylamine was converted to methane by the LCB24 culture. The production of $^{13}\text{CO}_2$ may represent
183 the dismutation of $^{13}\text{CH}_3\text{-NH}_2$ to generate reducing power for methanogenesis via the methyl-branch of the
184 Wood-Ljungdahl pathway or may be explained by other organisms in the culture catabolizing MMA. Yet,
185 no transcriptomic evidence for this activity was present in this experiment. No methane production was
186 observed for cultures treated with BES or in cultures incubated without MMA (Fig. 3D). When BES was
187 added to cultures in the exponential phase, methane production ceased indicating the generation of methane
188 is reliant on the *Archaeoglobi* MCR (Fig. 3E).

189

190 **Visualization and cell enumeration**

191 The growth of *Ca. M. hypatiae* was tracked in four replicates during the SIT experiment with
192 catalyzed reporter deposition fluorescence *in situ* hybridization (CARD-FISH) using a general archaea-
193 targeted probe Arch915 (36) and DNA-staining (DAPI) (Fig. 1C). As the production of methane increased
194 throughout the experiment, there was a concurrent rise in the relative cell abundance of *Ca. M. hypatiae*
195 (Fig. 3F, SI Appendix, Table S5). The initial assessment on day 22 across four replicates revealed the total
196 cell density to be $3.45 \times 10^7 \pm 1.14 \times 10^7$ before substantial concentrations of methane had been detected in
197 the headspace ($<132 \mu\text{M}$). By day 32, methane concentrations reached $1,777 \pm 739 \mu\text{M}$ and the total cell
198 density increased to $6.97 \times 10^7 \pm 3.73 \times 10^7 \text{ cells mL}^{-1}$ with 54% ($\pm 9.6\%$) of cells labeled as *Ca. M. hypatiae*
199 (Fig. 3F). All but one of these replicates were then sacrificed for further analysis. Finally on day 45, the
200 remaining replicate reached a headspace methane concentration of $4,109 \mu\text{M}$ and a total cell density of 1.22
201 $\times 10^8$ with 53% of cells labeled as *Ca. M. hypatiae*.

202 Visualization of the enrichment culture via scanning electron microscopy (SEM) revealed that most
203 cells exhibited a regular to irregular coccoid morphology, with a width ranging from $0.5\text{-}1 \mu\text{m}$ (Fig. 1D).
204 This morphology has previously been described for other *Archaeoglobi* species (30, 37-39).

205

206 **Alternative Substrates and Temperature Optimum**

207 We determined the substrate and temperature range of *Ca. M. hypatiae* by growing the culture in the
208 presence of several substrates at $70 \text{ }^\circ\text{C}$ or with 10 mM MMA at $60\text{-}85 \text{ }^\circ\text{C}$ (Fig. 4AB). Conditions that lead
209 to the production of methane included $10 \text{ mM trimethylamine (TMA)}$, $10 \text{ mM dimethylamine (DMA)}$, 10
210 mM MMA in media without yeast extract, and the control with 10 mM MMA and 0.01% yeast extract.
211 Methane production of cultures grown with MMA in the presence or absence of yeast extract were
212 indistinguishable ($5,202 \pm 606$ and $5,703 \pm 410 \mu\text{M CH}_4$, respectively) indicating that yeast extract is not
213 essential for methanogenic growth. Observed methane concentrations were higher in incubations amended
214 with DMA ($10,115 \pm 836 \mu\text{M CH}_4$) and TMA ($9,524 \pm 3,626 \mu\text{M CH}_4$, with a wide range of $5,361\text{-}11,993$
215 μM) on average more than the MMA controls, consistent with what has been observed for other
216 methylotrophic methanogens (40). Incubations amended with $10 \text{ mM methanol (MeOH)}$ did not produce
217 methane after 47 days of incubation at $70 \text{ }^\circ\text{C}$. Due to its use by sulfate reducing organisms as an electron

218 donor (41), 10 mM lactate (LAC) was tested, as well as 10 mM MMA with 10 mM LAC, but none of these
219 incubations produced methane. Production of methane has not been observed in any attempted transfers
220 where only hydrogen (99.9999% purity) was present in the headspace, or hydrogen with MMA was added
221 (data not shown).

222 The enrichment grew optimally at both 64 and 70 °C with relative amounts of methane produced at
223 5,304±451 µM and 5,202±606 µM, respectively. This is in contrast to the predicted optimal growth
224 temperature of 74.4°C deduced from the *Ca. M. hypatiae* MAG via Tome (42). This is lower than the
225 observed range of growth and optimum temperatures for type strains of non-methanogenic Archaeoglobus
226 which have been demonstrated to grow between 50 and 95 °C with optimal temperatures between 75-83 °C
227 in organisms sourced predominantly from deep sea vent environments (30). No methane production was
228 detected at temperatures 77 °C or above or lower than 64 °C after 47 days of incubation (Dataset S4).

229

230 Genomic and Transcriptomic Basis for Methanogenesis

231 The assembled metagenome obtained at the end of the SIT experiment was used to align a total of
232 23,376,154 million metatranscriptome mRNA reads obtained from six replicates harvested in the
233 exponential growth phase and to create a detailed reconstruction of the metabolism of *Ca. M. hypatiae* (Fig.
234 3AB, 5, Dataset S5). A total of 22,891,651 reads, *i.e.*, 97.8% of all recovered reads, were recruited to the
235 *Ca. M. hypatiae* MAG. Only 2.1% of the total mRNA reads (484,503) were aligned with other co-enriched
236 organisms. Among these, only 13 genes across four MAGs were expressed above 200 RPKM and just five
237 genes exceeded >1,000 RPKM. Notably, genes required for the conversion of methylamine to methane
238 were among the top 2% of highest expressed genes transcribed by *Ca. M. hypatiae*, including genes
239 encoding the MCR complex (*mcrAGCDB*; 15,976 RPKM), monomethylamine methyltransferase (*mtmB*;
240 884-9,884 RPKM), dimethylamine corrinoid (*mtbC*; 3,677 RPKM), and methanol:coenzyme M
241 methyltransferase (*mtaA*; 12,577 RPKM) (Fig. 5). Seven copies of substrate-specific methyltransferases for
242 MMA (*mtmB*; 3 copies), DMA (*mtbB*; 2 copies), and TMA (*mttB*; 2 copies) were present in the genome,
243 but methanol methyltransferase (*mtaB*) was not identified. These genes were differentially expressed with
244 one copy for each type of methylamine expressed above 3,200 RPKM. In addition to *mtbC*, two gene copies
245 of the trimethylamine corrinoid protein (*mttC*) were found in the genome but their expression was relatively
246 low (<460 RPKM average). Monomethylamine corrinoid (*mtmC*) or methanol corrinoid (*mtaC*) proteins
247 were not identified in *Ca. M. hypatiae*. Additionally, genes were expressed for pyrrolysine synthesis
248 (*pylBCD*; 819, 343, 37 RPKM) and the methyltransferase corrinoid activation protein (*ramA*; 1,076
249 RPKM), both of which support methylamine methyltransferases in methylotrophic methanogenesis (43,
250 44). The absence of *mtmC* and the high expression levels of *mtbC* (3,677 RPKM) and *mtaA* (12,577 RPKM)
251 suggests that they are responsible for the transfer of a methyl group from monomethylamine to coenzyme
252 M (CoM) after it has been transferred by a substrate-specific methyltransferase (*mtmB*). Consistent with
253 the observed methane production from DMA and TMA, *Ca. M. hypatiae* can use these methylamines and
254 expressed the corresponding genes (*mtbB*, *mttB*) at comparatively high levels (JOOIALLP_01813 *mtbB*
255 3,249 RPKM; JOOIALLP_01787 *mttB* 5,324 RPKM; Fig. 4B, 5). It is worth noting that the expression of
256 these genes was detected despite the culture not having been previously exposed to DMA or TMA at the
257 time of the transcriptomics experiment. We hypothesize that *Ca. M. hypatiae* could employ one of two
258 strategies: it either (i) constitutively expresses all substrate-specific methyltransferases and corrinoid
259 proteins as a precautionary measure to accommodate substrates potentially encountered *in situ*, or (ii) *Ca.*
260 *M. hypatiae* transcriptionally co-regulates the genes responsible for these functions.

261 *Ca. M. hypatiae* expressed the methyl-branch of the Wood-Ljungdahl pathway (WLP) and the acetyl-
262 CoA decarbonylase/synthase complex (Cdh, *cdhABCDE*), which is consistent with genes observed and
263 shown to be expressed in sulfate-reducing Archaeoglobi genomes (41). This includes two paralogous copies
264 of 5,10-methylenetetrahydromethanopterin reductase (*mer*) which might function as a traditional Mer,
265 considering that these genes are also members of the large luciferase-like monooxygenase family
266 (pfam00296)(35). The expression of genes in the WLP varied. Methylenetetrahydromethanopterin
267 dehydrogenase (*mtd*), methenyltetrahydromethanopterin cyclohydrolase (*mch*), formylmethanofuran-
268 tetrahydromethanopterin N-formyltransferase (*ptr*), formylmethanofuran dehydrogenase (*fwdABC*), and
269 one copy of the *mer* homologs were expressed at comparatively high levels (456-2,763 RPKM), while
270 FwdDEFG and the other *mer* copy were only minimally expressed (<180 RPKM). The high expression of
271 the Cdh complex (*cdhACDE*; 3,063±362, *cdhB* 677 RPKM average across subunits) suggests that *Ca. M.*
272 *hypatiae* is capable of autotrophically fixing CO₂ to acetyl-CoA as has been shown for other *Archaeoglobus*
273 species (45). Acetyl-CoA could also be derived from the degradation of fatty acids present in yeast extract
274 through the process of beta-oxidation. Enzymes involved in this pathway were expressed at moderate to
275 high levels during growth (340-3,864 RPKM). Pyruvate synthase (Por) was highly expressed providing a
276 way for acetyl-CoA to be converted to pyruvate and subsequently be fed into major biosynthetic pathways.
277 Specifically, *Ca. M. hypatiae* encodes pyruvate carboxylase (PycAB), an incomplete reductive
278 tricarboxylic acid cycle (rTCA), phosphoenolpyruvate synthase (Pps), most enzymes needed for
279 gluconeogenesis, and several enzymes associated with the pentose phosphate pathway in archaea, which
280 were all expressed at varying levels (Dataset S5). Together, these pathways provide *Ca. M. hypatiae* the
281 capacity to synthesize amino acids, carbohydrates, integral components of the cell wall, and vital sugars for
282 nucleic acids.

283 Several complexes related to energy conservation and electron transport were moderately to highly
284 expressed. *Ca. M. hypatiae* encodes a fused heterodisulfide reductase (*hdrDE*) that was highly expressed
285 (1,106±120 RPKM) in addition to a fused *hdrD/mvhD* and four copies of *hdrD* that were all expressed at
286 much lower levels (<500 RPKM). The differing levels of transcription suggest the membrane-bound HdrDE
287 is responsible for the regeneration of coenzymes M and B through the reduction of heterodisulfide (CoM-
288 S-S-CoB). Additionally, the absence of HdrB, which contains the active site for disulfide reduction,
289 eliminates the possibility that disulfide reduction could occur via a HdrABC complex (46). A unique gene
290 cluster was identified containing F₄₂₀-non-reducing hydrogenase (MvhAGD), two HdrA copies and a
291 QmoC fused to a HdrC. One HdrA copy (JOOIALLP_01710) was predicted by DiSCo analysis as a
292 quinone-modifying oxidoreductase (QmoB), a protein related to the HdrA of methanogens (47, 48). This
293 cluster was expressed at high levels (995-2,431 RPKM average), suggesting its importance for electron
294 transfer in *Ca. M. hypatiae*. We hypothesize these subunits are associating together *in vivo* to bifurcate
295 electrons from hydrogen (H₂) to reduce both menaquinone (MQ) and ferredoxin (Fd_{ox}), as proposed recently
296 (35, 49). Lastly, *Ca. M. hypatiae* moderately expressed a membrane-bound F₄₂₀H₂:quinone oxidoreductase
297 (Fqo) complex (88-280 RPKM across subunits) and a V-type ATP synthase (24-442 RPKM across
298 subunits).

299 The reductant required for reducing the CoM-S-S-CoB made during conversion of methylated
300 substrates to methane during methylotrophic methanogenesis can originate from two possible routes. The
301 first possibility would rely on sourcing electrons from hydrogen, which could be oxidized by the Mvh-
302 Qmo-Hdr complex coupled to menaquinone reduction. H₂ may be produced through the activity of a group
303 3b [NiFe]-sulfhydrogenase (HydABDG), which was the highest expressed hydrogenase complex with an
304 average RPKM of 4,421 across subunits (50, 51). To evolve hydrogen via HydABDG, reducing power, via

305 NADPH, could be supplied by sulfide dehydrogenase (SudAB; Sud A, 1,088 RPKM; SudB, 495 RPKM).
306 Alternatively, NADPH could instead be provided to biosynthesis pathways and therefore be decoupled
307 from methanogenic metabolism. H₂ could also potentially be sourced from fermentative bacteria in the
308 enrichment culture, however, the low number of hydrogenases encoded by co-enriched organisms were
309 only very lowly expressed at the time of sampling for metatranscriptomics (<51 RPKM). At this point, the
310 source of H₂ *Ca. M. hypatiae* uses remains uncertain, as no H₂ was added to the headspace. Second, in a
311 hydrogen-independent electron transport system, reduced F₄₂₀ and ferredoxin could be produced through
312 the dismutation of methylated substrate to CO₂ through the WLP. Reduced F₄₂₀ could be oxidized by the
313 Fqo complex and contribute to a reduced menaquinone pool that could be used by the fused HdrDE complex
314 to reduce CoM-S-S-CoB. Reduced ferredoxin could be oxidized at a soluble FqoF to reduce F₄₂₀ or at an
315 Fqo complex lacking FqoF to reduce menaquinone (52, 53). Based on the low expression levels of the Fqo
316 complex (171±67 RPKM) and the absence of F₄₂₀-reducing hydrogenase (*frh*) from the genome, it is not
317 likely the WLP runs in the reductive direction as a source of reduced F₄₂₀ would be required. Resolving the
318 exact configuration of the electron transport system encoded by *Ca. M. hypatiae* will require biochemical
319 confirmation in future investigations.

320 Importantly, genes necessary for dissimilatory sulfate reduction typically observed in sulfate-
321 reducing members of the Archaeoglobi, including dissimilatory sulfite reductase (*dsrAB*), sulfate
322 adenylyltransferase (*sat*), and adenylylsulfate reductase (*aprAB*), were neither identified in the genome of
323 *Ca. M. hypatiae* nor in the unbinned fraction of the metagenome. They were also absent from the
324 comparatively incomplete MAG of *Ca. M. nevadensis* GBS (35). However, *Ca. M. hypatiae* encodes
325 subunits *dsrMK* and *dsrOP* of the Dsr complex in addition to *dsrC*. This complex is strictly conserved in
326 sulfate-reducing organisms (54) where it mediates electron transfer from the periplasm to the cytoplasm
327 reducing the disulfide bond found in DsrC cysteines (55). The expression of the Dsr complex and *dsrC* was
328 low (450±63 RPKM) during growth on monomethylamine suggesting it is not vital to the metabolism of
329 *Ca. M. hypatiae*. The presence of the Dsr complex, DsrC, and subunits QmoC and QmoB in the genome
330 may be explained as evolutionary remnants from ancestral Archaeoglobi, which initially grew as sulfate-
331 reducing organisms but later transitioned to a methanogenic lifestyle (7, 8). This raises the question whether
332 intermediate of this process, Archaeoglobi capable of both methanogenesis and sulfate-reduction (and
333 possible anaerobic oxidation of methane), still exist today.

334 Collectively, the metagenomic and transcriptomic data confirmed that *Ca. M. hypatiae* is not only
335 the sole archaeon but the sole methanogen in our culture. The metabolic reconstruction and
336 metatranscriptomics results are consistent with methylotrophic methanogenesis from methylamines. The
337 absence of genes required for sulfate reduction eliminates the possibility for this metabolism in *Ca. M.*
338 *hypatiae*. A unique gene cluster (Mvh-Qmo-Hdr) potentially involved in energy conservation was
339 expressed, however future studies will be required to test how *Ca. M. hypatiae* internally cycles electrons
340 for methanogenesis and if it sources H₂, or other reductants, from the medium or co-enriched bacteria.

341

342 **Distribution of *Ca. Methanoglobus* Across Geothermal Features in YNP**

343 16S rRNA and *mcrA* gene amplicon sequence data generated in a recent microbial diversity survey
344 of 100 geothermal features in YNP (33) were used to analyze the distribution of Archaeoglobi related to
345 *Ca. M. hypatiae* (SI Appendix, Fig. S5). 16S rRNA gene amplicons closely related to *Ca. M. hypatiae*
346 (96.7-100% sequence identity) were found in seven DNA samples from six hot springs (pH 5.1-9.35, 31-
347 78 °C) in addition to hot spring LCB024 (the source of this culture) at relative abundances ranging from
348 0.02-0.22%. In addition, *mcrA* gene ASVs affiliated with Archaeoglobi were PCR-amplified from 53 DNA

349 samples. These were collected from microbial mats or sediments originating from 36 geothermal features
350 distributed across various thermal regions within YNP by Lynes, Krukenberg *et al.* (33). Archaeoglobi-
351 related *mcrA* genes were found in geothermal features with a pH range of 2.61 to 9.32 and a temperature
352 range of 18.4 °C to 93.8 °C. Collectively, our results and the studies by Wang *et al.* and Buessecker *et al.*,
353 who reported that Mcr-encoding Archaeoglobi are present (35) and transcriptionally active in hot spring
354 mesocosms (34), demonstrate the previously overlooked role Archaeoglobi might play in the anaerobic
355 carbon cycle of geothermal environments.

356

357 **Conclusion**

358 In summary, the cultivation of *Ca. Methanoglobus hypatiae* LCB24 provides direct experimental
359 evidence that members of the Archaeoglobi are methanogens. *Ca. M. hypatiae* can use MMA, DMA, and
360 TMA as methanogenic substrates and grows optimally at 64-70 °C, as evidenced by metagenomics,
361 metatranscriptomics, and isotope tracing experiments. Metagenomic sequencing and phylogenomic
362 analysis confirmed the close relationship of *Ca. M. hypatiae* to other Mcr-encoding Archaeoglobi and the
363 relatedness of its *mcrA* to MAGs of the TACK superphylum, some of which have recently been showed to
364 also be methanogens (56, 57). Together, this supports the idea that the capacity for methanogenesis is deeply
365 rooted in the archaea and possibly dates to the last common ancestor of archaea (1, 3, 7, 8, 58). The wide
366 distribution of Archaeoglobi-affiliated *mcrA* gene sequences and *Ca. M. hypatiae*-related 16S rRNA gene
367 sequences in geothermal features across YNP suggests that members of this lineage play a hitherto
368 unaccounted-for role in anaerobic carbon cycling in these extreme ecosystems. Future studies of *Ca. M.*
369 *hypatiae* and other methanogens will provide valuable insights into the evolution of methane metabolism
370 and the significance of these archaea in biogeochemical cycles across geothermal and other environments.

371

372 **Materials and Methods**

373 All chemicals used in this study were sourced from Sigma Aldrich unless otherwise specified.

374

375 **Sample Collection, Enrichment, and Cultivation**

376 In November 2021, a slurry of sediment and water (1:9) was collected from an unnamed hot spring
377 in the Lower Culex Basin of Yellowstone National Park (YNP), WY, USA. In our previous survey of Mcr-
378 encoding archaea in YNP (33), this hot spring was given the identifier LCB024 (44.573294, -110.795388;
379 pH 7.8, 67 °C). A mixture of surface sediment (~1-2 cm deep) and hot spring water was collected into a
380 glass bottle and sealed headspace-free with a thick butyl rubber stopper. Collected material was transported
381 back to the lab and stored at room temperature. Using this material as inoculum, 30 mL enrichments were
382 established in February 2022 in 60 mL serum bottles. Material was homogenized by mixing and was then
383 diluted 1:10 (v/v) with anoxic medium in an anoxic glove box (N₂/CO₂/H₂; 90/5/5%).

384 Medium was prepared anoxically as described previously (59) and contained a base of (per liter):
385 KH₂PO₄, 0.5 g; MgSO₄·7H₂O, 0.4 g; NaCl, 0.5 g; NH₄Cl, 0.4 g; CaCl₂·2H₂O, 0.05 g; HEPES, 2.38 g; yeast
386 extract, 0.1 g; and 0.002% (w/v) (NH₄)₂Fe(SO₄)₂·6H₂O, 5 mM NaHCO₃, 1 mL trace element solution SL-
387 10, 1 mL Selenite-Tungstate solution, 1 mL CCM vitamins (60), 0.0005% (w/v) resazurin, 10 mg of
388 coenzyme-M, 2 mg sodium dithionite, 1 mM dithiothreitol, 1 mM Na₂S·9H₂O, with pH adjusted to 7.8.
389 Serum bottles were sealed with butyl rubber stoppers and aluminum crimps before the headspace was
390 exchanged with N₂ (99.999%) for 5 minutes and set to a 200 kPa N₂ atmosphere. Monomethylamine
391 (MMA) was added from a filter-sterilized methylamine-hydrochloride anoxic stock solution to a final
392 concentration of 10 mM. The bacterial antibiotics streptomycin (50 mg/L; inhibitor of protein synthesis)

393 and vancomycin (50 mg/L; inhibitor of peptidoglycan synthesis) were added from filter-sterilized anoxic
394 stock solutions. The enrichments were incubated at 70 °C in the dark without shaking. Cultures were
395 maintained by regular transfer of 10% v/v into fresh media, which contained MMA and antibiotics. A
396 sediment-free culture was obtained after the third transfer after which it was transferred at 10% v/v to 50
397 mL in 125 mL serum bottles.

398

399 **Stable Isotope Tracing**

400 The conversion of ¹³C- or D₃-MMA (¹³CH₃-NH₂, CD₃-NH₂) to ¹³CH₄ or CD₃H was tracked by
401 incubating active enrichment cultures in the presence of 20% labeled substrate (98%; Cambridge Isotope
402 Laboratories). Incubations were carried out in 30 mL culture volumes in 60 mL serum bottles with 8% v/v
403 inoculum, 50 mg/L streptomycin, 50 mg/L vancomycin, 10 mM MMA, and N₂ gas (99.999%) incubated in
404 anoxic media (pH 7.8, 70 °C) in six replicates (SI Appendix, Fig. S3). Duplicate control incubations
405 included (i) ¹²C-MMA and (ii) inoculum without MMA. Triplicate control incubations were performed with
406 (iii) ¹²C-MMA plus 10 mM bromoethanesulfonate (BES) added in mid-exponential phase (day 33) to inhibit
407 methanogenesis and (iv) 10 mM BES added at time of inoculation (day 0) without substrate. Headspace
408 samples were collected throughout the experiment as described above and analyzed using a Shimadzu
409 QP2020 NX GCMS equipped with a GS-CarbonPLOT column (30 m × 0.35 mm; 1.5 μm film thickness;
410 Agilent) and operated in Selected Ion Monitoring mode. The instrument was operated using the method
411 described in Ai et al., 2013 (61) with helium as a carrier gas. Peak areas corresponding to m/z ratios of 16
412 for ¹²CH₄, 17 for ¹³CH₄, and 19 for CD₃H were used for quantification.

413

414 **Metagenomic Sequencing, Assembly, and Annotation**

415 Two metagenomes were obtained over the course of this study. A 42 mL aliquot of the fourth transfer
416 of the enrichment (Fig. 1 T4-MG) was filtered onto a 0.22 μm filter, transferred to a lysing matrix E tube,
417 and DNA extracted immediately following filtration. Genomic DNA was extracted using the FastDNA Spin
418 Kit for Soil (MP Biomedicals, Irvine, CA) following the manufacturer's guidelines.

419 A second metagenome was recovered from one of the six culture replicates grown in the presence of
420 CD₃-NH₂ and used for recruiting transcriptomic reads from the other replicates (Fig. 1 SIT-MG). A 60 mL
421 syringe flushed with N₂ gas was used to transfer 30 mL of culture to a sterilized oak ridge tube. Cells were
422 harvested through centrifugation for 30 minutes at 10,000 rpm at 4 °C. The supernatant was removed, and
423 DNA extracted from the pellet using the FastDNA Spin Kit for Soil (MP Biomedicals, Irvine, CA)
424 following the manufacturer's guidelines.

425 Genomic DNA for both metagenomes was shipped to SeqCenter (Pittsburgh, PA) and sample
426 libraries were prepared using the Illumina DNA Prep kit and 10bp unique dual indices (UDI). The first
427 metagenome (T4-MG) was sequenced on an Illumina NextSeq 2000 and the second (SIT-MG) sequenced
428 on an Illumina NovaSeq 6000, each producing 2x151bp reads. Demultiplexing, quality control, and adapter
429 trimming was performed with bcl-convert v3.9.3. Quality of the reads were evaluated with FastQC before
430 quality, linker and adapter trimming, artifact and common contaminate removal, and error correction were
431 performed with the rqcfilter2 pipeline (maxn=3, maq=10, trimq=15 (first dataset), trimq=20 (second
432 dataset)) and bbcm (mincount=2, hcf=0.6). Resulting reads were assembled with SPAdes v3.15.13 (Nurk,
433 2017) (-k 33,55,77,99,127 --meta --only-assembler) and coverage was determined with bbmap
434 (ambiguous=random). Combined assemblies were performed with the trimmed and error corrected reads
435 and the same assembly parameters, or with the raw reads but excluding the --only-assembler option.
436 Annotation of the assembled sequences was performed with Prokka v1.14.16 (62). Assembled scaffolds

437 ≥ 2000 bp were binned using Maxbin v2.2.7 (63), Metabat v2.12.1 (with and without coverage) (64),
438 Concoct v1.0.0 (65), Autometa v1 (bacterial and archaeal modes with the machine learning step) (66),
439 followed by bin refinement with DAS_Tool v1.1.6 (67), as previously described (68). Bin completeness
440 and redundancy were assessed with CheckM v1.2.2 (69).

441

442 **RNA Extraction, Sequencing, and Transcriptomic Processing**

443 Total RNA was extracted for transcriptomics from four of the six replicates of *Archaeoglobus*
444 cultivated in the presence of labeled substrate ($^{13}\text{CH}_3\text{-NH}_2$ or $\text{CD}_3\text{-NH}_2$) for a total of eight replicates. Each
445 replicate culture in the exponential growth phase (day 32) was moved from the 70 °C incubator to an ice
446 bath placed at -20 °C for 40 minutes to stop cellular activity. A 60 mL syringe flushed with N_2 gas was used
447 to transfer 30 mL of culture to a sterilized oak ridge tube and kept on ice. Cells were harvested through
448 centrifugation for 30 minutes at 10,000 rpm at 4 °C. The supernatant was removed, and the pellet transferred
449 to a lysing matrix E tube (MP Biomedicals, Irvine, CA) to which 600 μL of RNA lysis buffer was added.
450 Samples were homogenized in a MP Bioscience FastPrep instrument for 40 seconds at a speed setting of
451 6.0 m/s followed by centrifugation for 15 minutes at 14,000 rpm. RNA was extracted using the Quick-RNA
452 miniprep kit (Zymo Research, Irvine, CA) including a DNase treatment step and eluted in 50 μL of RNase
453 free water. Centrifugation steps were performed at 15,000 rpm and the final spin for elution at 10,000 rpm.
454 Of the eight replicates extracted, six measured >50 ng/ μL ($3\times$ $^{13}\text{CH}_3\text{-NH}_2$ and $3\times$ $\text{CD}_3\text{-NH}_2$) and were sent
455 for transcriptomic sequencing at SeqCenter (Pittsburgh, PA). Samples were DNase treated with Invitrogen
456 DNase (RNase free). Library preparation was performed using Illumina's Stranded Total RNA Prep
457 Ligation with Ribo-Zero Plus kit and 10bp UDI. Sequencing was done on a NovaSeq 6000, producing
458 paired end 151bp reads. Demultiplexing, quality control, and adapter trimming was performed with bcl-
459 convert (v4.1.5). Read quality was further evaluated with FastQC v0.11.9 (70) before quality trimming and
460 artifact, rRNA, and common contaminant removal with the rqcfilter2 pipeline (trimq=28, maxns=3,
461 maq=20), and error correction with bbcms (mincount=2, hcf=0.6) from the BBTools suite v38.94 (71).
462 BBMap: a fast accurate, splice-aware aligner. <https://sourceforge.net/projects/bbmap>). Additional rRNA
463 gene reads were detected and removed with Ribodetector v0.2.7 (72) and any remaining rRNA gene reads
464 were finally removed with bbmap, using rRNA genes recovered from the metagenomes (see below) as
465 references. The resulting mRNA reads were mapped against annotated genes from the paired metagenomes
466 with bbmap (ambig=random).

467

468 **Data Availability**

469 All metagenomic, metatranscriptomic, and amplicon data discussed in this manuscript are available
470 under NCBI BioProject ID PRJNA1014417. McrA gene amplicon data from YNP hot springs discussed in
471 this manuscript has been previously published (Lynes et al., 2023) and is available under NCBI under
472 BioProject PRJNA859922.

473

474 **Acknowledgements**

475 This study was funded through a NASA Exobiology program award (80NSSC19K1633) to R.H. We
476 thank the US National Park Service for permitting work in YNP under permit number YELL-SCI-8010.
477 We thank George Schaible (MSU) for help with SEM imaging, Dr. Viola Krukenberg (MSU) for initial
478 FISH methodology development, Sylvia Nupp, Dr. Andrew Montgomery, and Paige Schlegel (all MSU)
479 for assistance with field sampling, Dr. Christopher Lemon (MSU) for allowing use of his cooling centrifuge,
480 and Dr. Marike Palmer (UN Las Vegas) for discussing naming of this archaeon.

481 **References**

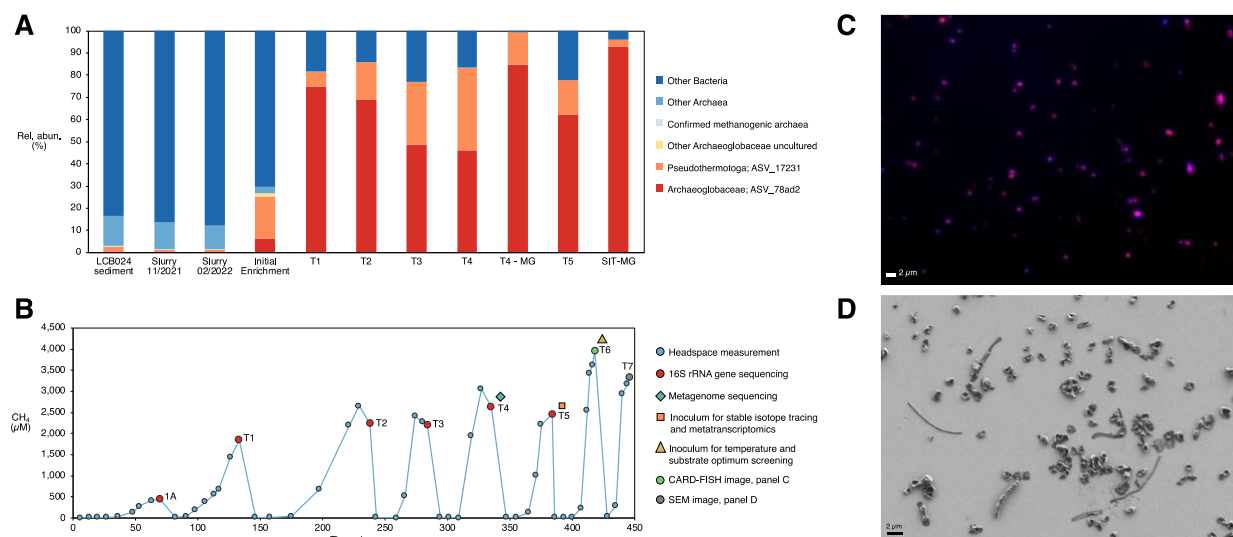
- 482 1. J. M. Wolfe, G. P. Fournier, Horizontal gene transfer constrains the timing of methanogen
483 evolution. *Nat Ecol Evol* **2**, 897-903 (2018).
- 484 2. D. Y. Sorokin *et al.*, Discovery of extremely halophilic, methyl-reducing euryarchaea
485 provides insights into the evolutionary origin of methanogenesis. *Nat Microbiol* **2**, 17081
486 (2017).
- 487 3. W. F. Martin, F. L. Sousa, Early Microbial Evolution: The Age of Anaerobes. *Cold Spring
488 Harb Perspect Biol* **8**, a018127 (2015).
- 489 4. B. Sauterey, B. Charnay, A. Affholder, S. Mazevet, R. Ferrière, Co-evolution of primitive
490 methane-cycling ecosystems and early Earth's atmosphere and climate. *Nature
491 Communications* **11**, 2705 (2020).
- 492 5. Y. Ueno, K. Yamada, N. Yoshida, S. Maruyama, Y. Isozaki, Evidence from fluid
493 inclusions for microbial methanogenesis in the early Archaean era. *Nature* **440**, 516-519
494 (2006).
- 495 6. A. Spang, T. J. G. Ettema, Archaeal evolution: The methanogenic roots of Archaea. *Nature
496 Microbiology* **2**, 17109 (2017).
- 497 7. P. S. Adam, G. E. Kolyfets, T. L. V. Bornemann, C. E. Vorgias, A. J. Probst, Genomic
498 remnants of ancestral methanogenesis and hydrogenotrophy in Archaea drive anaerobic
499 carbon cycling. *Science Advances* **8**, eabm9651 (2022).
- 500 8. Y. Wang *et al.*, A methylotrophic origin of methanogenesis and early divergence of
501 anaerobic multicarbon alkane metabolism. *Science Advances* **7**, eabj1453 (2021).
- 502 9. K.-U. Hinrichs, Microbial fixation of methane carbon at 2.7 Ga: Was an anaerobic
503 mechanism possible? *Geochemistry, Geophysics, Geosystems* **3**, 1-10 (2002).
- 504 10. M. Saunois *et al.*, The Global Methane Budget 2000–2017. *Earth Syst. Sci. Data* **12**, 1561-
505 1623 (2020).
- 506 11. J. A. Rosentreter *et al.*, Half of global methane emissions come from highly variable
507 aquatic ecosystem sources. *Nature Geoscience* **14**, 225-230 (2021).
- 508 12. P. S. Garcia, S. Gribaldo, G. Borrel, Diversity and Evolution of Methane-Related Pathways
509 in Archaea. *Annual Review of Microbiology* **76**, null (2022).
- 510 13. J. G. Ferry, K. A. Kstead, "Methanogenesis" in Archaea. (2007),
511 <https://doi.org/10.1128/9781555815516.ch13>, pp. 288-314.
- 512 14. R. Conrad, The global methane cycle: recent advances in understanding the microbial
513 processes involved. *Environ Microbiol Rep* **1**, 285-292 (2009).
- 514 15. S. Scheller, M. Goenrich, R. Boecher, R. K. Thauer, B. Jaun, The key nickel enzyme of
515 methanogenesis catalyses the anaerobic oxidation of methane. *Nature* **465**, 606-608
516 (2010).
- 517 16. R. K. Thauer, Methyl (Alkyl)-Coenzyme M Reductases: Nickel F-430-Containing
518 Enzymes Involved in Anaerobic Methane Formation and in Anaerobic Oxidation of
519 Methane or of Short Chain Alkanes. *Biochemistry* **58**, 5198-5220 (2019).
- 520 17. P. N. Evans *et al.*, An evolving view of methane metabolism in the Archaea. *Nat Rev
521 Microbiol* **17**, 219-232 (2019).
- 522 18. R. K. Thauer, A. K. Kaster, H. Seedorf, W. Buckel, R. Hedderich, Methanogenic archaea:
523 ecologically relevant differences in energy conservation. *Nat Rev Microbiol* **6**, 579-591
524 (2008).
- 525 19. B. J. Baker *et al.*, Diversity, ecology and evolution of Archaea. *Nat Microbiol* **5**, 887-900
526 (2020).

- 527 20. C. P. Bueno de Mesquita, D. Wu, S. G. Tringe, Methyl-Based Methanogenesis: an
528 Ecological and Genomic Review. *Microbiol Mol Biol Rev* **87**, e0002422 (2023).
- 529 21. A. Söllinger, T. Urich, Methylotrophic methanogens everywhere — physiology and
530 ecology of novel players in global methane cycling. *Biochemical Society Transactions* **47**,
531 1895-1907 (2019).
- 532 22. M. K. Nobu, T. Narihiro, K. Kuroda, R. Mei, W. T. Liu, Chasing the elusive Euryarchaeota
533 class WSA2: genomes reveal a uniquely fastidious methyl-reducing methanogen. *ISME J*
534 **10**, 2478-2487 (2016).
- 535 23. I. Vanwonterghem *et al.*, Methylotrophic methanogenesis discovered in the archaeal
536 phylum Verstraetearchaeota. *Nat Microbiol* **1**, 16170 (2016).
- 537 24. L. J. McKay *et al.*, Co-occurring genomic capacity for anaerobic methane and dissimilatory
538 sulfur metabolisms discovered in the Korarchaeota. *Nat Microbiol* **4**, 614-622 (2019).
- 539 25. Y. Wang, G. Wegener, J. Hou, F. Wang, X. Xiao, Expanding anaerobic alkane metabolism
540 in the domain of Archaea. *Nat Microbiol* **4**, 595-602 (2019).
- 541 26. P. N. Evans *et al.*, Methane metabolism in the archaeal phylum Bathyarchaeota revealed
542 by genome-centric metagenomics. *Science* **350** (2015).
- 543 27. B. A. Berghuis *et al.*, Hydrogenotrophic methanogenesis in archaeal phylum
544 Verstraetearchaeota reveals the shared ancestry of all methanogens. *Proc Natl Acad Sci U*
545 *SA* **116**, 5037-5044 (2019).
- 546 28. Y. F. Liu *et al.*, Genomic and Transcriptomic Evidence Supports Methane Metabolism in
547 Archaeoglobi. *mSystems* **5** (2020).
- 548 29. K. O. Stetter, G. Lauerer, M. Thomm, A. Neuner, Isolation of Extremely Thermophilic
549 Sulfate Reducers: Evidence for a Novel Branch of Archaeobacteria. *Science* **236**, 822-824
550 (1987).
- 551 30. G. Slobodkina *et al.*, Physiological and Genomic Characterization of a Hyperthermophilic
552 Archaeon *Archaeoglobus neptunius* sp. nov. Isolated From a Deep-Sea Hydrothermal Vent
553 Warrants the Reclassification of the Genus *Archaeoglobus*. *Front Microbiol* **12**, 679245
554 (2021).
- 555 31. J. A. Boyd *et al.*, Divergent methyl-coenzyme M reductase genes in a deep-subseafloor
556 Archaeoglobi. *ISME J* **13**, 1269-1279 (2019).
- 557 32. Z. S. Hua *et al.*, Insights into the ecological roles and evolution of methyl-coenzyme M
558 reductase-containing hot spring Archaea. *Nat Commun* **10**, 4574 (2019).
- 559 33. M. M. Lynes *et al.*, Diversity and function of methyl-coenzyme M reductase-encoding
560 archaea in Yellowstone hot springs revealed by metagenomics and mesocosm experiments.
561 *ISME Communications* **3**, 22 (2023).
- 562 34. J. Wang *et al.*, Evidence for nontraditional mcr-containing archaea contributing to
563 biological methanogenesis in geothermal springs. *Science Advances* **9**, eadg6004 (2023).
- 564 35. S. Buessecker *et al.*, Mcr-dependent methanogenesis in Archaeoglobaceae enriched from
565 a terrestrial hot spring. *The ISME Journal* 10.1038/s41396-023-01472-3 (2023).
- 566 36. D. A. Stahl, Development and application of nucleic acid probes in bacterial systematics.
567 *Nucleic Acid Techniques in Bacterial Systematics*, 205-248 (1991).
- 568 37. K. O. Stetter, *Archaeoglobus fulgidus* gen. nov., sp. nov.: a new taxon of extremely
569 thermophilic archaeobacteria. *Syst. Appl. Microbiol.* **10**, 172-173 (1988).
- 570 38. H. Huber, H. Jannasch, R. Rachel, T. Fuchs, K. O. Stetter, *Archaeoglobus veneficus* sp.
571 nov., a Novel Facultative Chemolithoautotrophic Hyperthermophilic Sulfite Reducer,

- 572 Isolated from Abyssal Black Smokers. *Systematic and Applied Microbiology* **20**, 374-380
573 (1997).
- 574 39. K. Mori, A. Maruyama, T. Urabe, K.-i. Suzuki, S. Hanada, Archaeoglobus infectus sp.
575 nov., a novel thermophilic, chemolithoheterotrophic archaeon isolated from a deep-sea
576 rock collected at Suiyo Seamount, Izu-Bonin Arc, western Pacific Ocean. *International*
577 *Journal of Systematic and Evolutionary Microbiology* **58**, 810-816 (2008).
- 578 40. A. J. Watkins, E. G. Roussel, G. Webster, R. J. Parkes, H. Sass, Choline and N,N-
579 dimethylethanolamine as direct substrates for methanogens. *Appl Environ Microbiol* **78**,
580 8298-8303 (2012).
- 581 41. W. P. Hocking, R. Stokke, I. Roalkvam, I. H. Steen, Identification of key components in
582 the energy metabolism of the hyperthermophilic sulfate-reducing archaeon Archaeoglobus
583 fulgidus by transcriptome analyses. *Frontiers in microbiology* **5**, 95 (2014).
- 584 42. G. Li, K. S. Rabe, J. Nielsen, M. K. Engqvist, Machine learning applied to predicting
585 microorganism growth temperatures and enzyme catalytic optima. *ACS synthetic biology*
586 **8**, 1411-1420 (2019).
- 587 43. A. Mahapatra *et al.*, Characterization of a Methanosarcina acetivorans mutant unable to
588 translate UAG as pyrrolysine. *Mol Microbiol* **59**, 56-66 (2006).
- 589 44. T. Ferguson, J. A. Soares, T. Lienard, G. Gottschalk, J. A. Krzycki, RamA, a protein
590 required for reductive activation of corrinoid-dependent methylamine methyltransferase
591 reactions in methanogenic archaea. *J Biol Chem* **284**, 2285-2295 (2009).
- 592 45. S. Estelmann *et al.*, Carbon dioxide fixation in 'Archaeoglobus lithotrophicus': are there
593 multiple autotrophic pathways? *FEMS microbiology letters* **319**, 65-72 (2011).
- 594 46. J. G. Ferry, How to make a living by exhaling methane. *Annu Rev Microbiol* **64**, 453-473
595 (2010).
- 596 47. N. A. Chernyh *et al.*, Dissimilatory sulfate reduction in the archaeon 'Candidatus
597 Vulcanisaeta moutnovskia' sheds light on the evolution of sulfur metabolism. *Nat*
598 *Microbiol* **5**, 1428-1438 (2020).
- 599 48. S. Neukirchen, F. L. Sousa, DiSCo: a sequence-based type-specific predictor of Dsr-
600 dependent dissimilatory sulphur metabolism in microbial data. *Microbial Genomics* **7**
601 (2021).
- 602 49. A. R. Ramos, K. L. Keller, J. D. Wall, I. A. C. Pereira, The membrane QmoABC complex
603 interacts directly with the dissimilatory adenosine 5' -phosphosulfate reductase in sulfate
604 reducing bacteria. *Frontiers in microbiology* **3**, 137 (2012).
- 605 50. M. W. W. Adams, The metabolism of hydrogen by extremely thermophilic, sulfur-
606 dependent bacteria. *FEMS Microbiology Reviews* **6**, 219-237 (1990).
- 607 51. K. Ma, R. N. Schicho, R. M. Kelly, M. Adams, Hydrogenase of the hyperthermophile
608 Pyrococcus furiosus is an elemental sulfur reductase or sulfhydrogenase: evidence for a
609 sulfur-reducing hydrogenase ancestor. *Proceedings of the National Academy of Sciences*
610 **90**, 5341-5344 (1993).
- 611 52. W. P. Hocking, I. Roalkvam, C. Magnussen, R. Stokke, I. H. Steen, Assessment of the
612 Carbon Monoxide Metabolism of the Hyperthermophilic Sulfate-Reducing Archaeon
613 Archaeoglobus fulgidus VC-16 by Comparative Transcriptome Analyses. *Archaea* **2015**,
614 235384 (2015).
- 615 53. C. Welte, U. Deppenmeier, Membrane-bound electron transport in Methanosaeta
616 thermophila. *J Bacteriol* **193**, 2868-2870 (2011).

- 617 54. I. A. Pereira, S. A. Haveman, G. Voordouw, Biochemical, genetic and genomic
618 characterization of anaerobic electron transport pathways in sulphate-reducing delta-
619 proteobacteria. *Sulphate-Reducing Bacteria: Environmental and Engineered Systems (LL,
620 B. and WA, H., eds.)*, Cambridge University Press, Cambridge, UK (2007).
- 621 55. F. Grein, I. A. Pereira, C. Dahl, Biochemical characterization of individual components of
622 the Allochromatium vinosum DsrMKJOP transmembrane complex aids understanding of
623 complex function in vivo. *Journal of bacteriology* **192**, 6369-6377 (2010).
- 624 56. K. Wu *et al.*, Isolation of a methyl-reducing methanogen outside the Euryarchaeota.
625 (2023).
- 626 57. A. Kohtz *et al.*, Cultivation and visualization of a methanogen of the phylum
627 Thermoproteota. (2023).
- 628 58. A. Spang, E. F. Caceres, T. J. G. Ettema, Genomic exploration of the diversity, ecology,
629 and evolution of the archaeal domain of life. *Science* **357** (2017).
- 630 59. R. Laso-Perez, V. Krukenberg, F. Musat, G. Wegener, Establishing anaerobic
631 hydrocarbon-degrading enrichment cultures of microorganisms under strictly anoxic
632 conditions. *Nat Protoc* **13**, 1310-1330 (2018).
- 633 60. A. Brandis, R. K. Thauer, Growth of Desulfovibrio species on hydrogen and sulphate as
634 sole energy source. *Microbiology* **126**, 249-252 (1981).
- 635 61. G. Ai, J. Zhu, X. Dong, T. Sun, Simultaneous characterization of methane and carbon
636 dioxide produced by cultured methanogens using gas chromatography/isotope ratio mass
637 spectrometry and gas chromatography/mass spectrometry. *Rapid Commun Mass Spectrom*
638 **27**, 1935-1944 (2013).
- 639 62. T. Seemann, Prokka: rapid prokaryotic genome annotation. *Bioinformatics* **30**, 2068-2069
640 (2014).
- 641 63. Y.-W. Wu, Y.-H. Tang, S. G. Tringe, B. A. Simmons, S. W. Singer, MaxBin: an automated
642 binning method to recover individual genomes from metagenomes using an expectation-
643 maximization algorithm. *Microbiome* **2**, 26 (2014).
- 644 64. D. D. Kang, J. Froula, R. Egan, Z. Wang, MetaBAT, an efficient tool for accurately
645 reconstructing single genomes from complex microbial communities. *PeerJ* **3**, e1165
646 (2015).
- 647 65. J. Alneberg *et al.*, Binning metagenomic contigs by coverage and composition. *Nat*
648 *Methods* **11**, 1144-1146 (2014).
- 649 66. I. J. Miller *et al.*, Autometa: automated extraction of microbial genomes from individual
650 shotgun metagenomes. *Nucleic Acids Res* **47**, e57 (2019).
- 651 67. C. M. K. Sieber *et al.*, Recovery of genomes from metagenomes via a dereplication,
652 aggregation and scoring strategy. *Nat Microbiol* **3**, 836-843 (2018).
- 653 68. A. J. Kohtz, Z. J. Jay, M. M. Lynes, V. Krukenberg, R. Hatzenpichler, Culexarchaeia, a
654 novel archaeal class of anaerobic generalists inhabiting geothermal environments. *ISME*
655 *Communications* **2**, 86 (2022).
- 656 69. D. H. Parks, M. Imelfort, C. T. Skennerton, P. Hugenholtz, G. W. Tyson, CheckM:
657 assessing the quality of microbial genomes recovered from isolates, single cells, and
658 metagenomes. *Genome Res* **25**, 1043-1055 (2015).
- 659 70. S. Andrews, F. Krueger, A. Seconds-Pichon, F. Biggins, S. Wingett (2015) FastQC. A
660 quality control tool for high throughput sequence data. Babraham Bioinformatics.
661 Babraham Inst.

- 662 71. B. Bushnell (2014) BBMap: a fast, accurate, splice-aware aligner. (Lawrence Berkeley
663 National Lab.(LBNL), Berkeley, CA (United States)).
- 664 72. Z.-L. Deng, P. C. Münch, R. Mreches, A. C. McHardy, Rapid and accurate identification
665 of ribosomal RNA sequences via deep learning. *Nucleic acids research* **50**, e60-e60 (2022).
666
667



668
 669 **Fig. 1.** Community composition and methane production of the methanogenic enrichment culture
 670 containing *Ca. Methanoglobus hypatiae* LCB24. (A) Relative abundance of 16S rRNA gene amplicons in
 671 the initial sediment from hot spring LCB024, the slurry collected in November 2021, slurry material used
 672 to initiate enrichments in February 2022, the initial enrichment, and five subsequent transfers (T1-T5) are
 673 shown. For comparison, the estimated relative abundance of two metagenomic samples (T4-MG and SIT-
 674 MG) is included. The metagenome recovered from a replicate from the stable isotope tracing experiment
 675 incubated in the presence of deuterated methylamine (SIT-MG) revealed *Ca. M. hypatiae* grew to 92.8%
 676 relative abundance during the experiment. The two most abundant ASVs across enrichment transfers are
 677 shown with other taxa collapsed. Other methanogenic archaea were not identified in the initial enrichment
 678 or in any subsequent transfers. Relative sequence abundance for all ASVs is reported in SI Appendix, Table
 679 S1. (B) Headspace methane produced over long-term cultivation. The time between transfers decreased
 680 while the average maximum concentration of methane increased over time. Culture 1A represents the initial
 681 enrichment. A history of methane measurements can be found in SI Appendix, Table S2. (C) Visualization
 682 of *Ca. M. hypatiae* cells at T6 labeled via CARD-FISH by the general archaea probe Arch915 (red). DAPI
 683 staining of cells is in blue. (D) Cell morphologies in enrichment culture LCB24 at T7 as observed by
 684 secondary electron microscopy.

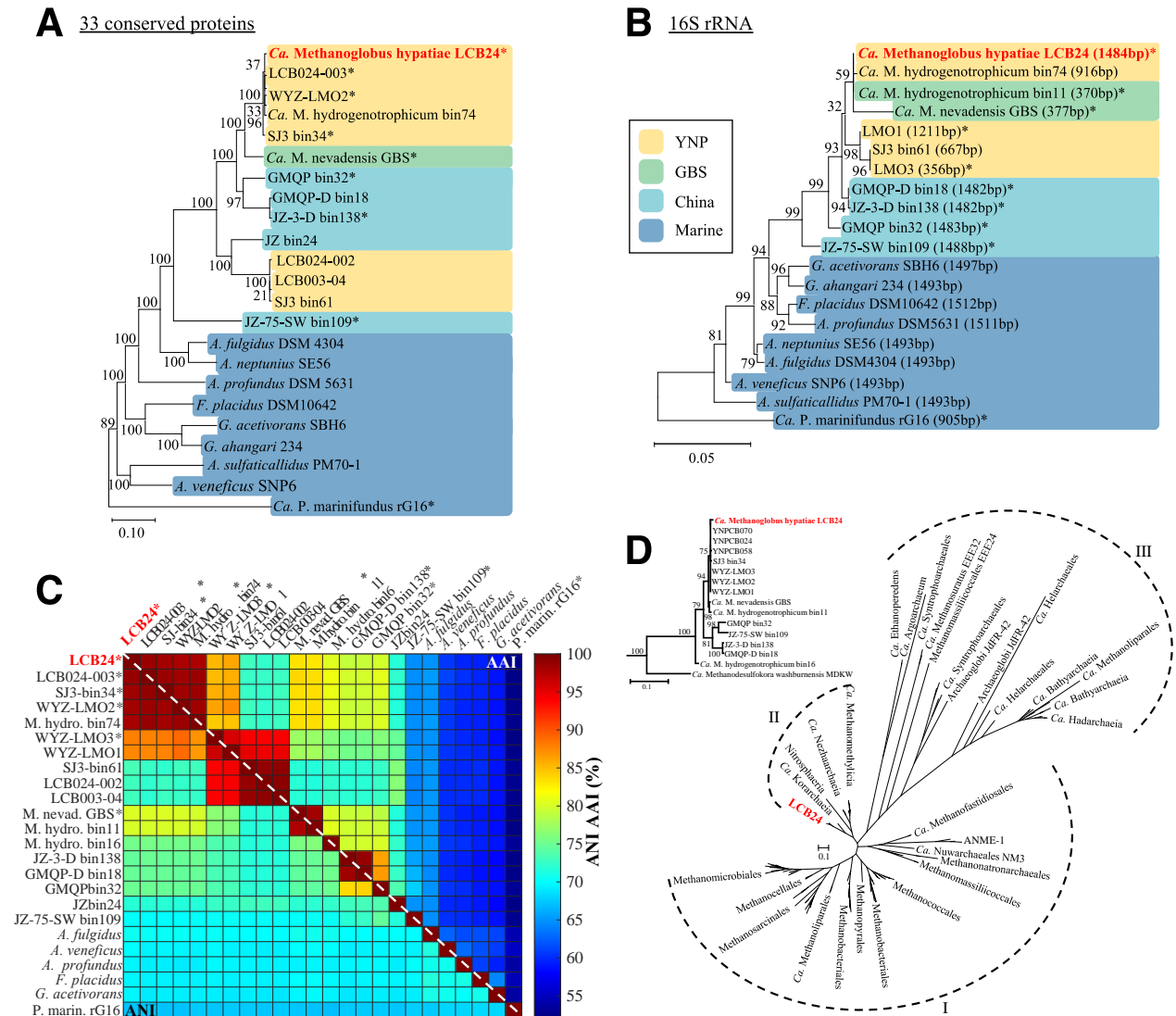


Fig. 2. Phylogenetic affiliation of *Ca. M. hypatiae* LCB24. (A) Maximum-likelihood tree, inferred with fasttree and WAG model (midpoint root), using a concatenated alignment of 33 conserved single copy proteins (list provided in SI Appendix, Table S4). References are colored by the habitat type from which sequences had been recovered: hot springs in Yellowstone National Park (YNP), yellow; Great Boiling Spring (GBS), green; hot springs in China, blue; marine hydrothermal vent systems, dark blue. (B) Maximum-likelihood tree inferred with fasttree using 16S rRNA genes with length in base pairs (bp). (C) ANI and AAI analysis of reference Archaeoglobales MAGs and genomes. Asterisks (*) indicate MAGs containing *mcrA*, apart from the MAG of *Ca. M. hydrogenotrophicum* bin74 which encodes a *mcrA* that is interrupted by a stop codon. AAI and ANI values are provided in SI Appendix, Fig. S1. (D) Maximum-likelihood tree, inferred with IQtree2 and the LG+C60+F+G model, from the amino acid alignment of McrA. Dashed lines indicate McrA/AcrA groups: (I) McrA from methanogens and ANME (MCR-type), (II) McrA from TACK lineages (MCR-type), (III) McrA-like from proposed and experimentally confirmed alkane oxidizing archaea (ACR-type). Insert shows MAGs closely related to *Ca. M. hypatiae* LCB24.

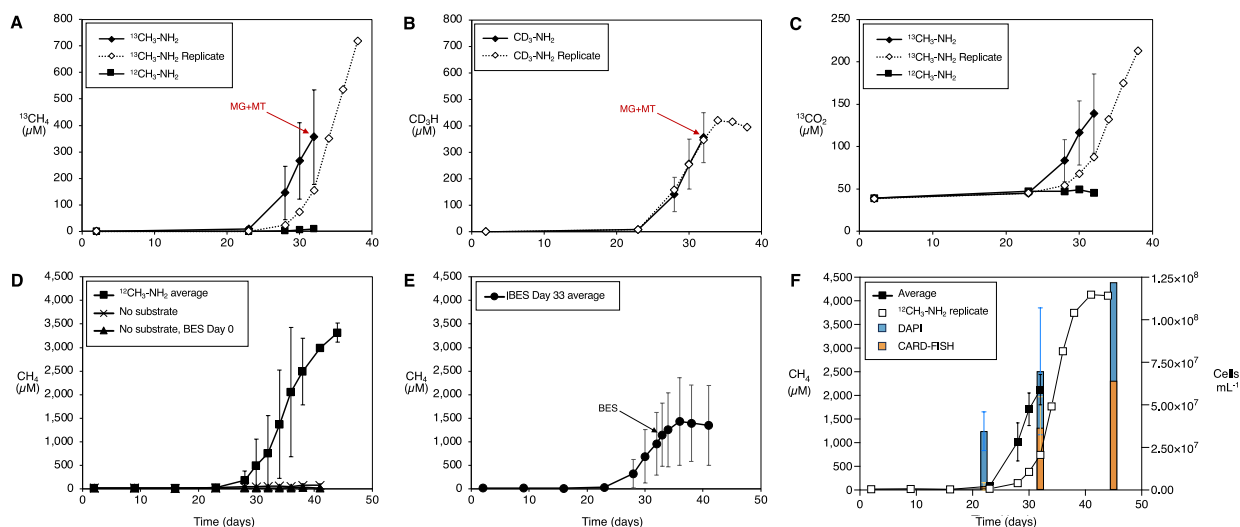


Fig. 3. Conversion of stable isotope labeled monomethylamine to methane by culture LCB24. (A) Production of $^{13}\text{CH}_4$ in cultures amended with $^{13}\text{CH}_3\text{-NH}_2$ vs. $^{12}\text{CH}_3\text{-NH}_2$ (6 replicates). (B) Production of CD_3H in cultures amended with $\text{CD}_3\text{-NH}_2$ (6 replicates). (C) Production of $^{13}\text{CO}_2$ in cultures amended with $^{13}\text{CH}_3\text{-NH}_2$ vs. $^{12}\text{CH}_3\text{-NH}_2$. For plots A and B, ten total replicates across treatments were sacrificed during mid-exponential phase for metagenomic or metatranscriptomic sequencing indicated by red arrows. $^{13}\text{CH}_4$, CD_3H , or $^{13}\text{CO}_2$ production for the replicate allowed to reach stationary phase is shown as a dashed line through open diamond symbols. (D) Production of $^{12}\text{CH}_4$ in cultures amended with ^{12}C -monomethylamine ($^{12}\text{CH}_3\text{-NH}_2$; 2 replicates). Cultures incubated without substrates (2 replicates) and those to which the inhibitor BES was added on day 0 (3 replicates) did not produce $^{12}\text{CH}_4$ over the course of the experiment. (E) Production of $^{12}\text{CH}_4$ in cultures amended with $^{12}\text{CH}_3\text{-NH}_2$ to which BES was added on day 33 of incubation (black arrow; 3 replicates). The average production of $^{12}\text{CH}_4$ leveled off and ceased after the introduction of BES, indicating methane generation by *Ca. M. hypatiae* is MCR-dependent. Error bars indicate standard deviation of biological replicates when applicable. Measurements of $^{12}\text{CH}_4$, $^{13}\text{CH}_4$, CD_3H , and $^{13}\text{CO}_2$ for all replicates and controls are reported in Dataset S2. $^{12}\text{CH}_4$ measurements for all controls and replicates are shown in SI Appendix, Fig. S4 and Dataset S3. (F) $^{12}\text{CH}_4$ production and fraction of *Ca. M. hypatiae* cells in biological replicates incubated with $^{13}\text{CH}_3\text{-NH}_2$. Relative abundance of cells was determined at three time points (day 22, 32, 45) based on the fraction of *Ca. M. hypatiae* specific CARD-FISH counts (orange) versus total counts of DAPI stained cells (blue). Error bars indicate the standard deviation for four biological replicates on days 22 and 32.

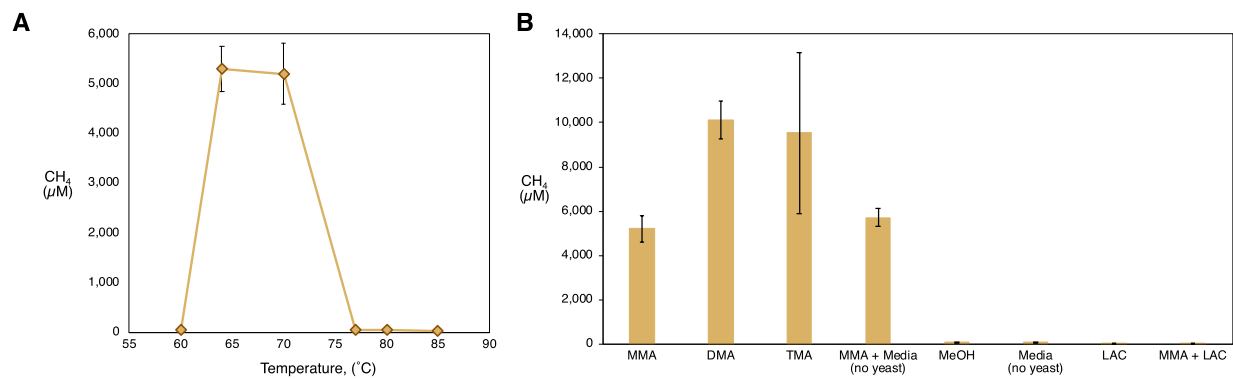


Fig. 4. Temperature and substrate range of culture LCB24. (A) Methane production from MMA was observed between 64-70 °C. (B) Substrate range. Methane production was observed for MMA, DMA, TMA, and in media prepared without yeast extract. LAC, lactate; MeOH, methanol. Both experiments performed in triplicate. All measurements can be found in Dataset S4.

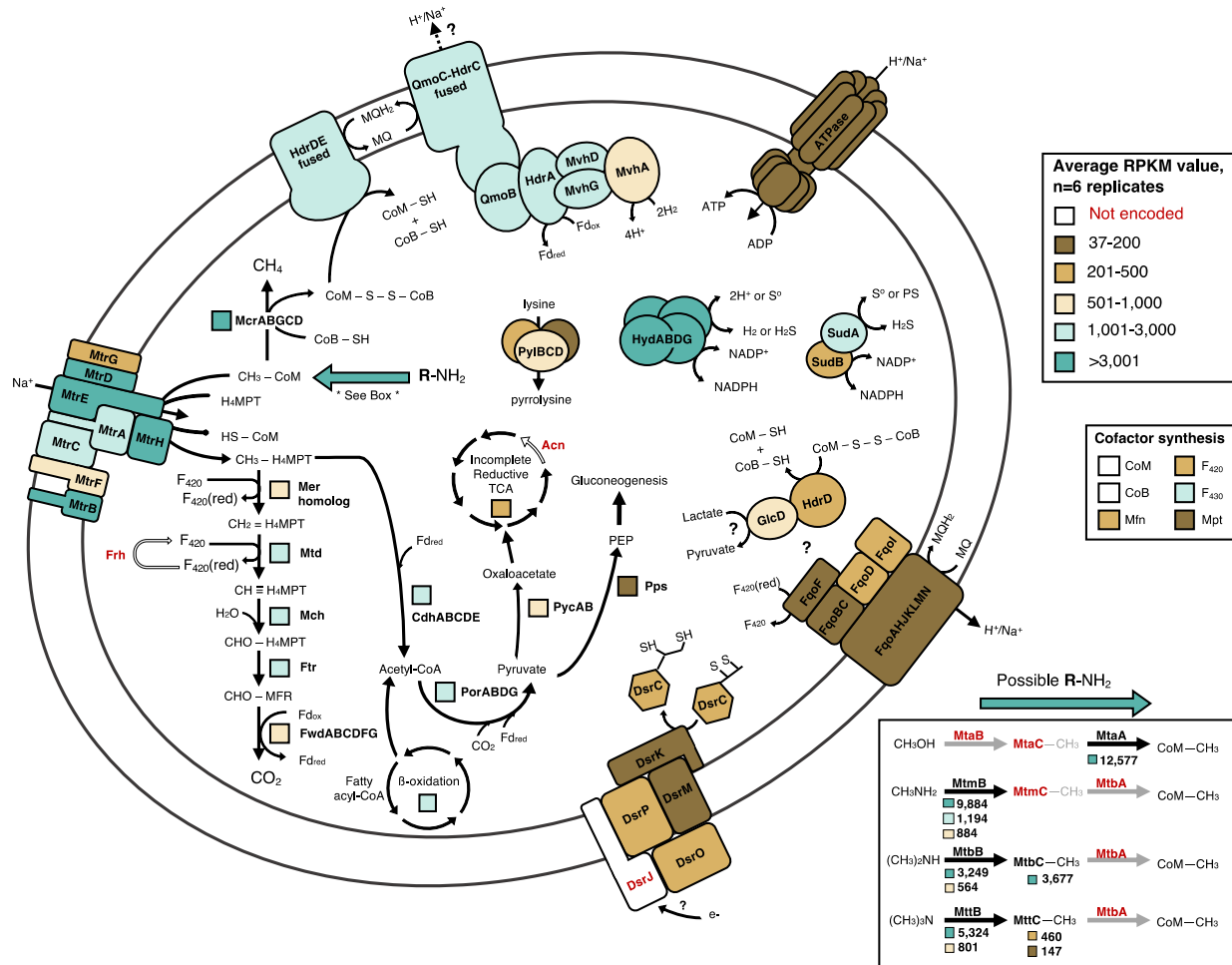


Fig. 5. Transcriptional activity in *Ca. M. hyatiae* grown under methanogenic conditions (N₂ headspace, 10 mM MMA, and 0.01% yeast extract). Transcriptionally active proteins are shown in bold black font. Proteins not encoded in the MAG are colored in white and denoted in bold red font. Average reads per kilobase of transcript per million mapped reads (RPKM) values of six biological replicates are depicted. RPKM values are represented by boxes or colored subunits close to each protein and are colored according to their expression level with the RPKM value of the lowest expressed gene depicted, 37 RPKM. For enzymes comprising multiple subunits, the beta-oxidation pathway, and the TCA cycle, an average RPKM value representing the transcribed enzymes is used. *Ca. M. hyatiae* is transcriptionally active under methanogenic conditions and encodes the ability to convert methyl-groups from mono-, di-, and trimethylamine to methane. This ability is enabled by several copies of substrate-specific methyltransferases and corrinoid proteins highlighted in the box to the bottom right. A complete list of genes described in this figure, their transcription levels, and their abbreviations is provided in Dataset S5.

1 **Supporting Information**

2

3 **SI Results and Discussion**

4 **Protologue**

5 *Methanoglobus hypatiae* sp. nov.

6 Me.tha.no.glo.bus. Gr. pref. *methano-*, pertaining to methane; L. masc. n. *-globus*, sphere; Gr.L.
7 masc. n. *Methanoglobus*, methane producing organism spherical in shape. This genus was named by
8 Buessecker *et al.* (1). Hy.pa.ti.ae. Gr. fem. hypatiae, to honor Hypatia of Alexandria, a respected and
9 renowned philosopher of ancient Alexandria, Egypt, who made significant contributions to the
10 understanding of mathematics and astronomy. A symbol of intellectual courage and scholarly achievement.
11 This archaeon was cultured from an unnamed hot spring in the Lower Culex Basin of Yellowstone National
12 Park identified as feature LCB024 (2). This archaeon is an obligately anaerobic thermophile that performs
13 methylotrophic methanogenesis using methylamines and grows as regular to irregular coccoid cells
14 approximately 0.5 to 1 μm in width. The type genome of this archaeon is deposited at NCBI under
15 BioProject PRJNA1014417, accession number will be added upon publication.

16

17 **SI Materials and Methods**

18 **Amplicon Sequencing and Analysis**

19 DNA was extracted from environmental slurry samples and enrichment cultures sampled on the day
20 of transfer using the FastDNA Spin Kit for Soil (MP Biomedicals, Irvine, CA) following the manufacturer's
21 guidelines. Archaeal and bacterial 16S rRNA genes were amplified with the updated Earth Microbiome
22 Project primer set 515F and 806R (3). Amplicon libraries were prepared as previously described (2) and
23 sequenced by the Molecular Research Core Facility at Idaho State University (Pocatello, ID) using an
24 Illumina MiSeq platform with 2 x 250 bp paired end read chemistry. Gene reads were processed using
25 QIIME 2 version 2022.8 (4). Primer sequences were removed from demultiplexed reads using cutadapt (5)
26 with error rate 0.12 and reads truncated (130 bp forward, 150 bp reverse), filtered, denoised and merged in
27 DADA2 with default settings (6). Processed 16S rRNA gene amplicon sequence variants (ASVs) were
28 taxonomically classified with the sklearn method and the SILVA 138 database (7). The R package
29 *decontam* (version 1.18.0) (8) was used to remove contaminants using the "Prevalence" model with a
30 threshold of 0.5.

31

32 **Annotation and Reconstruction of Metabolic Potential**

33 Genes associated with methanogenesis pathways, dissimilatory sulfur metabolism pathways,
34 coenzyme and cofactor biosynthesis, energy conservation, and beta-oxidation, were inventoried.
35 Annotations assigned by Prokka were refined through manual evaluation using KofamKOALA, NCBI
36 BLASTP, NCBI's Conserved Domain Database, InterPro, the hydrogenase classifier HydDB, and DiSCo
37 (9-14).

38

39 **Phylogenetic and Phylogenomic Analyses**

40 Average nucleotide identities (ANI) of 16S rRNA genes were calculated with blastn, while ANI and
41 average amino acid identities (AAI) were calculated with pyani v02.2.12 (ANiB) and CompareM v0.0.23
42 (--fragLen 2000) (<https://github.com/dparks1134/CompareM>), respectively for selected Archaeoglobales
43 genomes and MAGs (Table 1). Phylogenetic analysis of 16S rRNA genes was performed with fasttree (15)
44 using masked alignments generated by ssu-align.

45 Phylogenomic analysis was performed with a concatenated muscle (16) alignments of 33 conserved
46 phylogenetically informative single copy proteins (SI Appendix, Table S4) and maximum likelihood
47 analysis with fasttree (WAG model). McrA alignments were performed with MAFFT-LINSi v7.522 (17),
48 trimmed with trimAL v1.4.rev22 (18) using a 0.5 gap threshold, and maximum likelihood trees were built
49 with IQTree2 v2.0.6 (19) using LG+C60+F+G model and 1,000 ultrafast bootstraps.

50

51 **Temperature and Substrate Optimum Experiments**

52 Methane production and growth of *Archaeoglobus* was evaluated at different temperatures and in the
53 presence of methylated substrates (i.e., methanol and mono-, di-, and trimethylamine), lactate, and media
54 prepared without yeast extract. The sixth transfer of the enrichment was used to inoculate triplicate 30 mL
55 serum bottles containing 15 mL of medium with 8% v/v inoculum, streptomycin (50 mg/L), vancomycin
56 (50 mg/L), and 10 mM of each substrate tested. Cultures were evaluated at 60 °C, 64 °C, 70 °C, 77 °C, 80
57 °C, and 85 °C with 10 mM MMA. Separately, we tested whether the culture would grow on the following
58 substrate (combinations): 10 mM dimethylamine (DMA); 10 mM trimethylamine (TMA); 10 mM methanol
59 (MeOH); 10 mM lactate (LAC); 10 mM MMA and 10 mM LAC); 10 mM MMA with media without yeast
60 extract; and a control in media without yeast or any methanogenic substrate. The 70 °C cultures amended
61 with 10 mM MMA served as the control. All incubations were performed in biological triplicate.

62

63 **Methane Measurements**

64 During cultivation, 250 µL subsamples of the headspace were taken using a gas tight syringe
65 (Hamilton) and injected into a 10 mL autosampler vial that had been sealed with grey chlorobutyl septa.
66 Samples were taken from the autosampler vials and injected into a Shimadzu 2020-GC gas chromatograph
67 equipped with a GS433 CarbonPLOT column (30 m x 0.32 mm; 1.5 µm film thickness; Agilent) and a Rt-
68 Q-BOND column (30 m x 0.32 mm; 1.5 µm film thickness; Restek) using helium as a carrier gas. The
69 injector, column, and flame ionization detector (FID) were maintained at 200 °C, 50 °C, and 240 °C,
70 respectively. Methane concentrations were calculated based on injection of a standard curve.

71

72 **Fluorescence *in situ* hybridization and cell counts**

73 Aliquots of enrichment cultures incubated with ¹³C-MMA during the SIT experiment were treated
74 with 2% paraformaldehyde (PFA) and fixed for 1 hr at room temperature. Following fixation, cells were
75 washed twice with 1x PBS, followed by centrifugation at 16,000 × g to remove the supernatant, resuspended
76 in 1x PBS, and stored at 4 °C. For direct cell counts, aliquots of fixed cell suspensions were filtered onto
77 polycarbonate filters (0.2 µm pore size, 25 mm diameter, GTTP Millipore, Germany) and air dried before
78 filter pieces were cut and embedded in 0.2% low melting agarose. We attempted to use the
79 *Archaeoglobales*-specific probe Arglo32 (20), however fluorescent signal was insufficient. Given *Ca. M.*
80 *hypatiae* was the sole archaeon in the enrichment culture, the relative abundance of *Ca. M. hypatiae* cells
81 was determined via catalyzed reporter deposition fluorescence *in situ* hybridization (CARD-FISH) using
82 the general archaea-targeted 16S rRNA oligonucleotide probe Arch915 (21). Total cell counts were based
83 on DNA-stained cells using DAPI (4,6-diamidino-2-phenylindole). CARD-FISH was performed as
84 previously described (22). Cell wall permeabilization was achieved with a brief treatment of 0.1 M HCl (1
85 min, RT) followed by treatment with 0.01 M HCl (15 min, RT). Endogenous peroxidases were inactivated
86 with 0.15% H₂O₂ in methanol (30 min, RT). A formamide concentration of 35% was used for all
87 hybridization reactions (2.5 hrs, 46°C). CARD was performed using Alexa Fluor 594 labeled tyramides for
88 30 min at 46°C. Following signal amplification, an additional washing step in 1x PBS was included to

89 reduce background fluorescence (15 min, RT, dark). Samples were stained with DAPI, embedded in
90 Citifluor-Vectashield, and enumerated using an epifluorescence microscope (Leica DM4B).

91

92 **Secondary electron microscopy**

93 An aliquot of the enrichment culture at transfer 7 (T7) was treated with 2% paraformaldehyde (PFA)
94 and fixed for 1 hr at room temperature. Following fixation, cells were washed twice through centrifugation
95 at $16,000 \times g$ to remove the supernatant, resuspended in 1x phosphate buffered saline (PBS), and stored at
96 4°C . Samples for imaging were prepared according to Schaible et al., 2022 (23). Briefly, a square coupon
97 of mirror-finished 304 stainless steel (25 mm diameter, 0.6 mm thickness) was purchased from Stainless
98 Supply (Monroe, NC). The coupon was cleaned by washing with a 1% solution of Tergazyme (Alconox,
99 New York, NY) and rinsed with Milli-Q water. The coupon was dried under compressed air and stored at
100 room temperature. 5 μL of fixed sample was spotted on the coupon and air-dried at 46°C for 3 min. The
101 coupon was then dried for 1 m each step in a successive ethanol series starting with 10% ethanol and
102 increasing by increments of 10% with the last step 90% ethanol. SEM images were captured using a Zeiss
103 (Jena, Germany) SUPRA 55VP field emission scanning electron microscope (FE-SEM). The microscope
104 was operated at 1 keV under a vacuum of 0.2–0.3 mPa, with a working distance of 5.4–6.2 mm at the
105 Imaging and Chemical Analysis Laboratory (ICAL) of Montana State University (Bozeman, MT). No
106 conductivity coating was applied before SEM analysis as the microscope was operated at 1 keV.

107

108 **SI Detailed Author contributions**

109 M.M.L. and R.H. developed the research project. M.M.L., Z.J.J., A.J.K, and R.H. designed
110 experiments. M.M.L. and A.J.K. conducted field sampling. M.M.L. performed cultivation, extracted DNA
111 for amplicon and metagenomic sequencing, extracted RNA for transcriptomic sequencing, and conducted
112 physiology and stable isotope experiments. A.J.K. developed GC/GCMS protocols and processed GCMS
113 samples. Z.J.J. processed and annotated metagenomic and transcriptomic data, assembled MAGs, mapped
114 transcripts, assigned taxonomy, constructed 16S rRNA gene phylogeny, and performed phylogenetic
115 analysis of MAGs. M.M.L. conducted phylogenetic analysis of amplicon data, refined gene annotations,
116 reconstructed, and interpreted the metabolic potential of *Ca. M. hypatiae* with insight from Z.J.J and A.J.K.
117 R.H. was responsible for funding and supervision of the project. M.M.L. and R.H. wrote the manuscript,
118 which was then edited by all authors.

SI Tables

Table S1. Extended community composition history of methanogenic enrichment cultures via estimated relative abundance (%) from 16S rRNA gene amplicon sequencing.

	LCB024 sediment	Slurry 11/2021	Slurry 02/2022	Initial Enrichment	T1	T2	T3	T4	T4 - MG	T5	SIT-MG
Archaeoglobaceae ASV_78ad2	0.46	0.32	0.02	6.42	74.8	68.9	48.5	46.0	84.7	62.2	92.8
Pseudothermotoga ASV_17231	2.14	1.06	1.08	18.93	6.8	17.1	28.5	37.4	14.5	15.7	3.2
Other Archaeoglobaceae uncultured	0.00	0.00	0.00	1.54	0.0	0.01	0.0	0.0	0.0	0.0	0.0
Confirmed methanogenic archaea	0.25	0.38	0.45	0.00	0.0	0.0	0.0	0.0	0.0	0.0	0.0
Other Archaea	13.51	11.87	10.49	2.67	0.0	0.0	0.0	0.04	0.0	0.0	0.0
Other Bacteria	83.63	86.37	87.95	70.44	18.4	14.1	23.1	16.5	0.8	22.1	4.0

Table S2. Methane production of the enrichment culture over time. T, transfer.

Culture ID	Days continuous	Days	CH ₄ (μM)	CH ₄ (mM)	CH ₄ (ppm)	CH ₄ (%)
1A – initial enrichment	6	6	4.91	0.00	118.67	0.01
	13	13	16.73	0.02	404.73	0.04
	20	20	12.98	0.01	314.13	0.03
	27	27	12.86	0.01	311.20	0.03
	36	36	32.92	0.03	796.48	0.08
	48	48	146.28	0.15	3538.80	0.35
	53	53	279.15	0.28	6753.17	0.68
	63	63	419.11	0.42	10139.33	1.01
	70	70	447.12	0.45	10816.36	1.08
T1	82	12	14.40	0.01	348.40	0.03
	91	21	50.85	0.05	1230.06	0.12
	98	27	198.41	0.20	4800.09	0.48
	106	35	390.47	0.39	9445.97	0.94
	113	42	565.32	0.57	13676.04	1.37
	117	46	688.44	0.69	16654.06	1.67
	126	55	1442.03	1.44	34885.74	3.49
	133	62	1844.13	1.84	44611.75	4.46
T2	146	7	15.22	0.02	368.32	0.04
	158	18	16.11	0.02	389.83	0.04
	175	34	49.40	0.05	1195.06	0.12
	197	57	680.54	0.68	16463.41	1.65
	221	81	2200.24	2.20	53227.90	5.32
	229	89	2654.34	2.65	64213.66	6.42
	238	98	2230.72	2.23	53964.66	5.40
T3	243	5	18.17	0.02	439.53	0.04
	259	21	10.70	0.01	258.82	0.03
	266	28	536.13	0.54	12969.71	1.30
	274	36	2413.23	2.41	58379.47	5.84
	280	42	2283.95	2.28	55253.34	5.53
	284	46	2193.96	2.19	53077.04	5.31
T4	294	10	17.36	0.02	420.07	0.04
	301	17	18.12	0.02	438.37	0.04
	309	25	12.51	0.01	302.54	0.03
	319	35	1944.01	1.94	47028.08	4.70
	327	43	3054.00	3.05	73881.94	7.39
	335	51	2619.45	2.62	63370.12	6.34
T5	347	10	13.41	0.01	324.42	0.03
	355	18	13.14	0.01	317.78	0.03
	365	28	137.59	0.14	3328.60	0.33
	371	34	1023.35	1.02	24756.27	2.48
	375	38	2218.75	2.22	53674.81	5.37
	384	46	2459.29	2.46	59493.85	5.95
T6	386	2	16.29	0.02	394.19	0.04
	393	9	21.33	0.02	516.14	0.05
	400	16	18.68	0.02	451.92	0.05
	407	23	245.86	0.25	5947.76	0.59
	412	28	2555.27	2.56	61815.61	6.18
	414	30	3432.93	3.43	83051.24	8.31
	416	32	3621.90	3.62	87623.79	8.76
	418	34	3942.97	3.94	95385.88	9.54
T7	428	9	34.33	0.03	830.38	0.08
	435	16	296.91	0.30	7182.55	0.72
	440	21	2931.05	2.93	70907.06	7.09
	444	25	3164.45	3.16	76553.52	7.66
	446	27	3338.04	3.34	80751.55	8.08

Table S3. Extended Archaeoglobales metagenome assembled genome and isolate genome statistics. A combined assembly of metagenomes from T4-MG and SIT-MG (Fig. 1A) for the *Ca. M. hypatiae* LCB24 MAG was used as it yielded an improved assembly. Len., length; Compl., completeness; Redun, redundancy; Strain Hetero., strain heterogeneity; pOGT, predicted optimal growth temperature. * stop codon interrupts *mcrA* sequence; ^a Both sequences 5' start; not identical; ^b Consists of 1 chromosome and 1 plasmid.

	Seqs	Len (Mb)	GC (%)	Compl. (%)	Redun. (%)	16S	tRNA	CDS	<i>mcrA</i>	CRISPRs	pOGT (°C)	Citation
<i>Ca. M. hypatiae</i> LCB24	19	1.624	46.12	100	1.31	1	44	1,760	1	2	74.44	This study
Archaeoglobales LCB024-003	179	1.157	45.72	88.48	1.31	0	31	1,226	1	1	73.90	Lynes, Krukenberg et al, 2023
Archaeoglobales WYZ-LMO2	220	1.514	45.92	97.6	0	0	40	1,614	1	2	72.40	Wang 2019
Archaeoglobales bin/74	127	1.547	45.63	92.81	1.31	1	34	1,679	0*	9	75.32	Liu 2020
Archaeoglobales SJ3.Bin34	73	1.468	46.00	98.69	0.65	0	39	1,581	1	2	73.13	Colman 2019
<i>Ca. Methanoglobus nevadensis</i> GBS	71	1.602	47.16	98.04	3.66	1	47	1,785	1	2	74.75	Peacock 2013
Archaeoglobales GMQP bin32	20	1.727	41.26	100	0.98	1	39	1,931	1	2	71.88	Hua 2019
Archaeoglobales GMQP_D bin 18	22	1.565	42.01	97.39	0.98	1	45	1,747	1	3	69.41	Wang 2023
Archaeoglobales JZ-3 D bin 138	32	1.550	42.08	99.35	1.31	1	43	1,701	1	2	69.11	Wang 2023
Archaeoglobales WYZ-LMO1	140	1.557	43.85	88.89	1.31	1	41	1,701	1	1	72.72	Wang 2019
Archaeoglobales WYZ-LMO3	135	1.568	43.93	88.03	1.96	2 ^a	35	1,670	1	2	73.09	Wang 2019
Archaeoglobales bin11	252	1.220	47.59	91.83	6.17	1	27	1,387	1	0	72.64	Liu 2020
Archaeoglobales bin16	46	1.668	45.49	96.51	1.31	0	41	1,864	1	2	72.69	Liu 2020
Archaeoglobales JZ bin24	35	1.492	44.66	99.35	1.31	0	44	1,642	0	2	68.52	unpublished
Archaeoglobales LCB024-002	66	1.334	42.28	97.39	0.03	0	41	1,459	0	0	73.46	Lynes et al, 2023
Archaeoglobales LCB003-04	128	1.335	42.27	96.73	1.96	0	38	1,447	0	0	73.71	Lynes et al, 2023
Archaeoglobales SJ3 bin61	45	1.270	41.68	89.54	0	1	40	1,392	0	0	73.34	Colman 2019
Archaeoglobales JZ_75 SW bin 109	16	1.562	39.48	99.35	0.65	1	45	1,762	1	5	74.34	Wang 2023
Archaeoglobales fulgidus DSM 4304	1	2.178	48.58	100	0	1	46	2,440	0	3	79.88	Klenk 1997
Archaeoglobales neptunius SE56	32	2.116	46.05	100	0	1	47	2,336	0	2	78.26	Slobodkina 2021
Archaeoglobales profundus DSM 5631	2 ^b	1.563	46.05	100	0	1	48	1,784	0	0	85.86	von Jan 2010
Ferroglobus placidus DSM 10642	1	2.196	44.14	100	0	1	49	2,467	0	1	83.83	Anderson 2011
Geoglobus acetivorans SBH6	1	1.861	46.84	99.84	0	1	48	2,168	0	6	78.22	Mardanov 2014
Geoglobus ahangari 234	1	1.770	53.11	100	0	1	46	1,985	0	7	84.11	Manzella 2015
Archaeoglobales sulfatallidus PM70-1	1	2.077	43.24	100	0	1	51	2,237	0	1	76.12	Stokke 2013
Archaeoglobales veneficus SNP6	1	1.902	47.05	99.35	0	1	46	2,055	0	2	76.18	Mukherjee 2017
Polytropus marinitfundus rG116	21	2.129	40.22	99.84	1.96	1	44	2,286	2	0	66.39	Boyd 2019

Table S4. Conserved single copy proteins used in phylogenomic analysis of MAGs and isolates.

arCOG	Gene	Product
arCOG00405	GRS1	Glycyl-tRNA synthetase (class II)
arCOG00779	RplO	Ribosomal protein L15
arCOG00785	RpmC	Ribosomal protein L29
arCOG01001	Map	Methionine aminopeptidase
arCOG01183	Kae1p/TsaD	Subunit of KEOPS complex, contains a domain with ASKHA fold and RIO-type kinase (AP-endonuclease activity)
arCOG01228	Ffh	Signal recognition particle GTPase
arCOG01722	RpsM/rps13p	Ribosomal protein S13
arCOG01758	RpsJ/rps10p	Ribosomal protein S10
arCOG04070	RplC	Ribosomal protein L3
arCOG04071	RplD	Ribosomal protein L4
arCOG04072	RplW	Ribosomal protein L23
arCOG04086	RpmD	Ribosomal protein L30
arCOG04087	RpsE	Ribosomal protein S5
arCOG04088	RplR	Ribosomal protein L18
arCOG04090	RplF/rpl6p	Ribosomal protein L6P
arCOG04091	RpsH/rps8p	Ribosomal protein S8
arCOG04094	RplX/rpl24p	Ribosomal protein L24
arCOG04095	RplN/rps14p	Ribosomal protein L14
arCOG04096	RpsQ/rps17p	Ribosomal protein S17
arCOG04097	RpsC/rps3p	Ribosomal protein S3
arCOG04098	RplV/rpl22p	Ribosomal protein L22
arCOG04113	RplP	Ribosomal protein L10AE/L16
arCOG04121	RnhB	Ribonuclease HII
arCOG04169	SecY	Preprotein translocase subunit SecY
arCOG04185	RpsO	Ribosomal protein S15P
arCOG04239	RpsD/rps4p	Ribosomal protein S4 or related protein
arCOG04242	RplM/rpl13p	Ribosomal protein L13
arCOG04243	RpsI/rps9p	Ribosomal protein S9
arCOG04245	RpsB/rps2p	Ribosomal protein S2
arCOG04255	RpsL/rps12p	Ribosomal protein S12
arCOG04256	RpoC/Rpo11	DNA-directed RNA polymerase subunit A''
arCOG04257	RpoC/Rpo3/rpoA1	DNA-directed RNA polymerase subunit A'
arCOG04277	Efp	Translation elongation factor P (EF-P)/translation initiation factor 5A (eIF-5A)

Table S5. Calculated cell density of replicates in the SIT experiment. FID measurements of replicates used to determine cell density. Density is calculated based on cell counts of DAPI and CARD-FISH labeled samples. Stdev., standard deviation. Letters A-F identify each replicate.

Summary	¹² CH ₄		Cell Density, cells mL ⁻¹		% labeled with Arch915
	μM	ppm	DAPI	FISH	
5A Day 22	25	610	3.83 × 10 ⁷	1.34 × 10 ⁶	3.5
5B Day 22	57	1,374	1.88 × 10 ⁷	5.07 × 10 ⁶	12.7
5E Day 22	50	1,204	3.49 × 10 ⁷	0	0
5F Day 22	132	3,196	4.59 × 10 ⁷	2.21 × 10 ⁶	4.8
Day 22 Average	66	1,596	3.45 × 10 ⁷	2.16 × 10 ⁶	5.3
Day 22 Stdev.	46	1,116	1.14 × 10 ⁷	2.15 × 10 ⁶	5.4
5A Day 32	741	17,917	4.26 × 10 ⁷	2.85 × 10 ⁷	66.9
5B Day 32	2,176	52,635	1.11 × 10 ⁸	6.00 × 10 ⁷	54.2
5E Day 32	1,779	43,035	3.40 × 10 ⁷	1.74 × 10 ⁷	51.2
5F Day 32	2,412	58,355	9.14 × 10 ⁷	4.03 × 10 ⁷	44.1
Day 32 Average	1,777	42,985	6.97 × 10 ⁷	3.65 × 10 ⁷	54.1
Day 32 Stdev.	739	17,868	3.73 × 10 ⁷	1.82 × 10 ⁷	9.6
5A Day 45	4,109	99,398	12.2 × 10 ⁷	6.41 × 10 ⁷	52.7

SI Figures

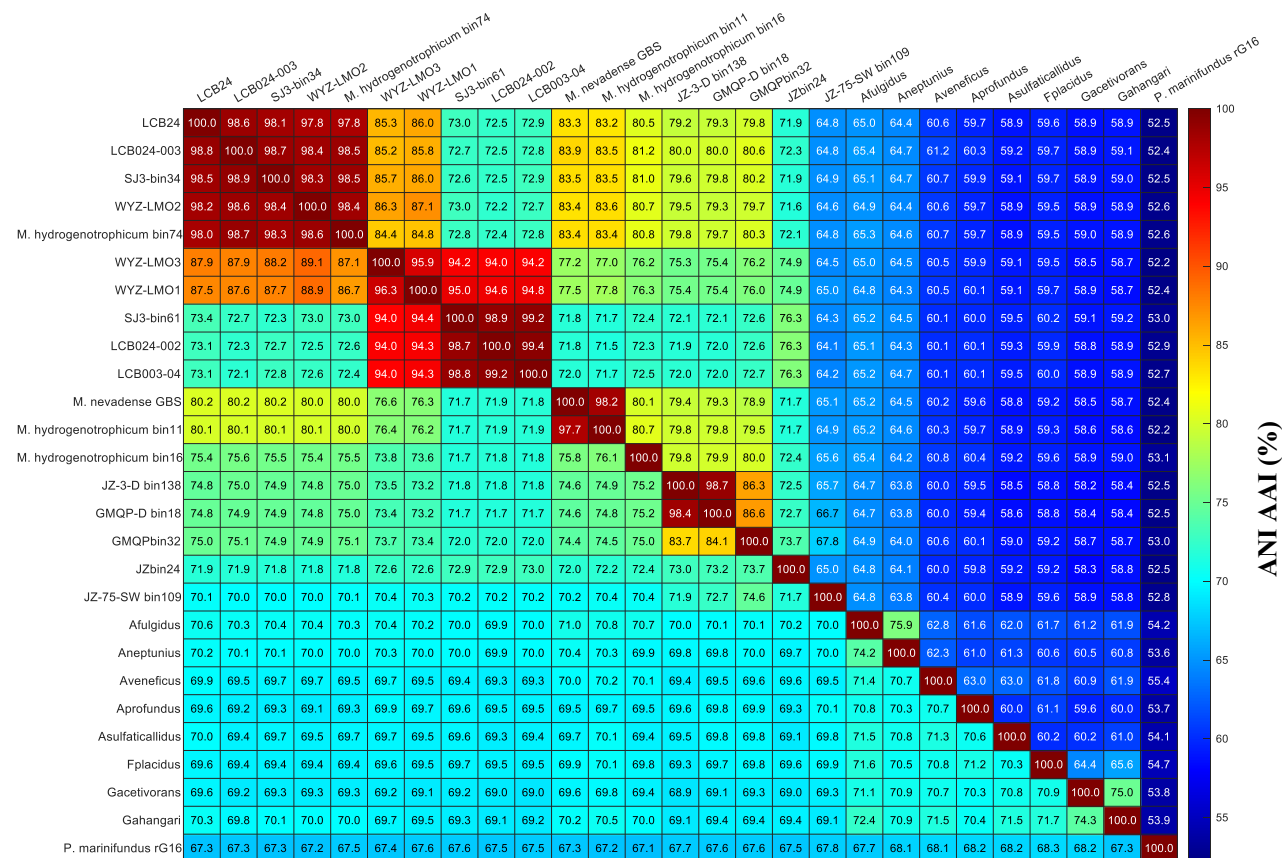


Fig. S1. Detailed ANI (lower half of matrix) and AAI (upper half of matrix) analysis of related Archaeoglobales MAGs and reference genomes.

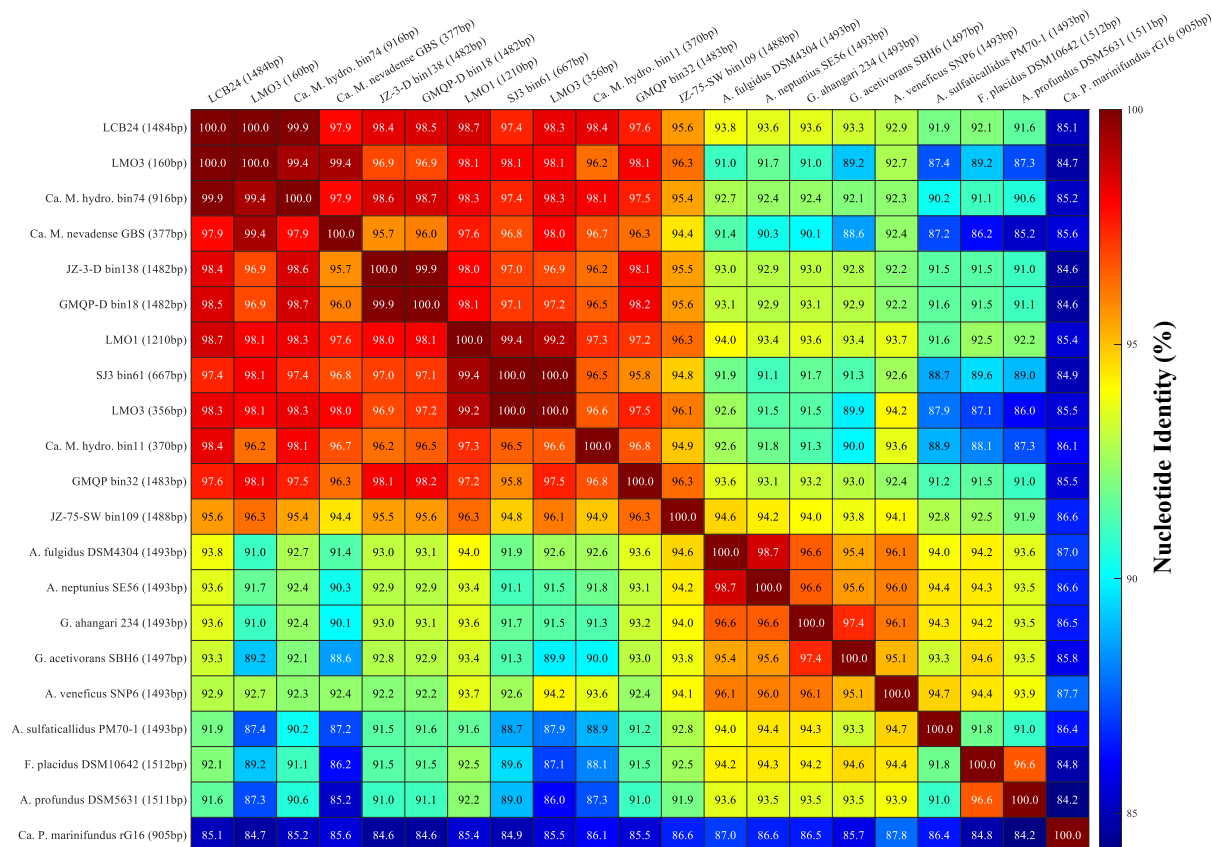


Fig. S2. 16S rRNA nucleotide identity analysis of closely related Archaeoglobales MAGs and reference genomes.

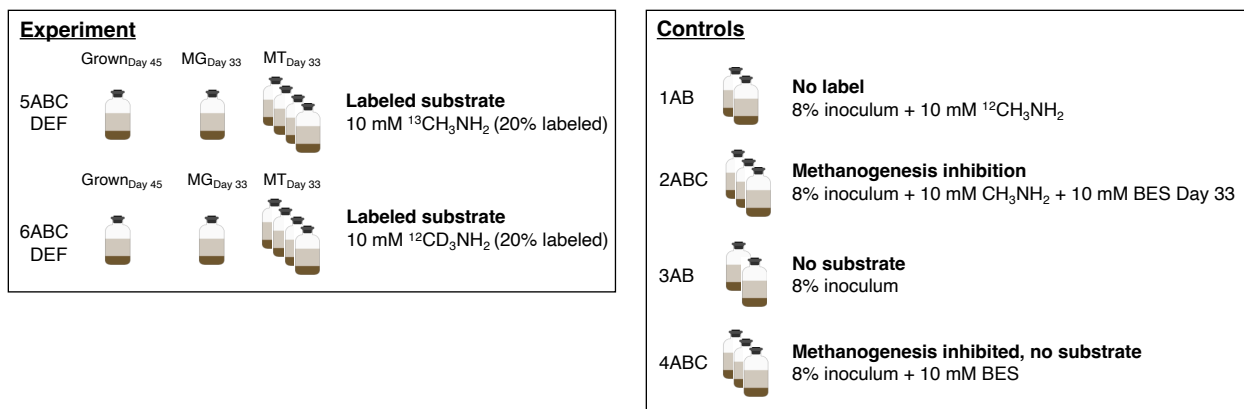


Fig. S3. Experimental setup of the stable isotope tracing (SIT) experiment. Replicates sacrificed for analysis during mid-log phase are indicated. Of the eight samples harvested for metatranscriptomics, six were sequenced and used for analysis as two replicates did not yield sufficient RNA for sequencing. MG, metagenome sample; MT, metatranscriptome sample; BES, bromoethanesulfonate/methanogenesis inhibitor.

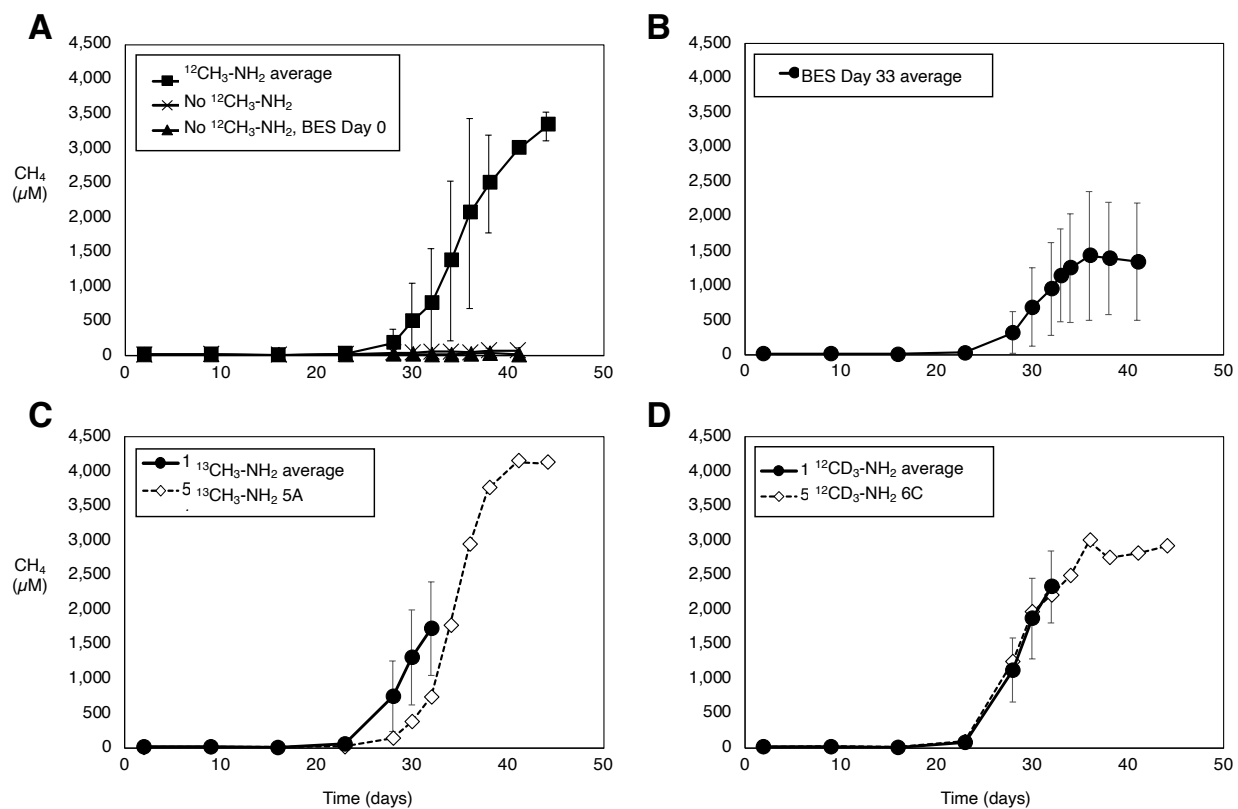


Fig. S4. ¹²CH₄ measurements by GC-FID during the stable isotope tracing experiment. Measurements can be found in Dataset S3.

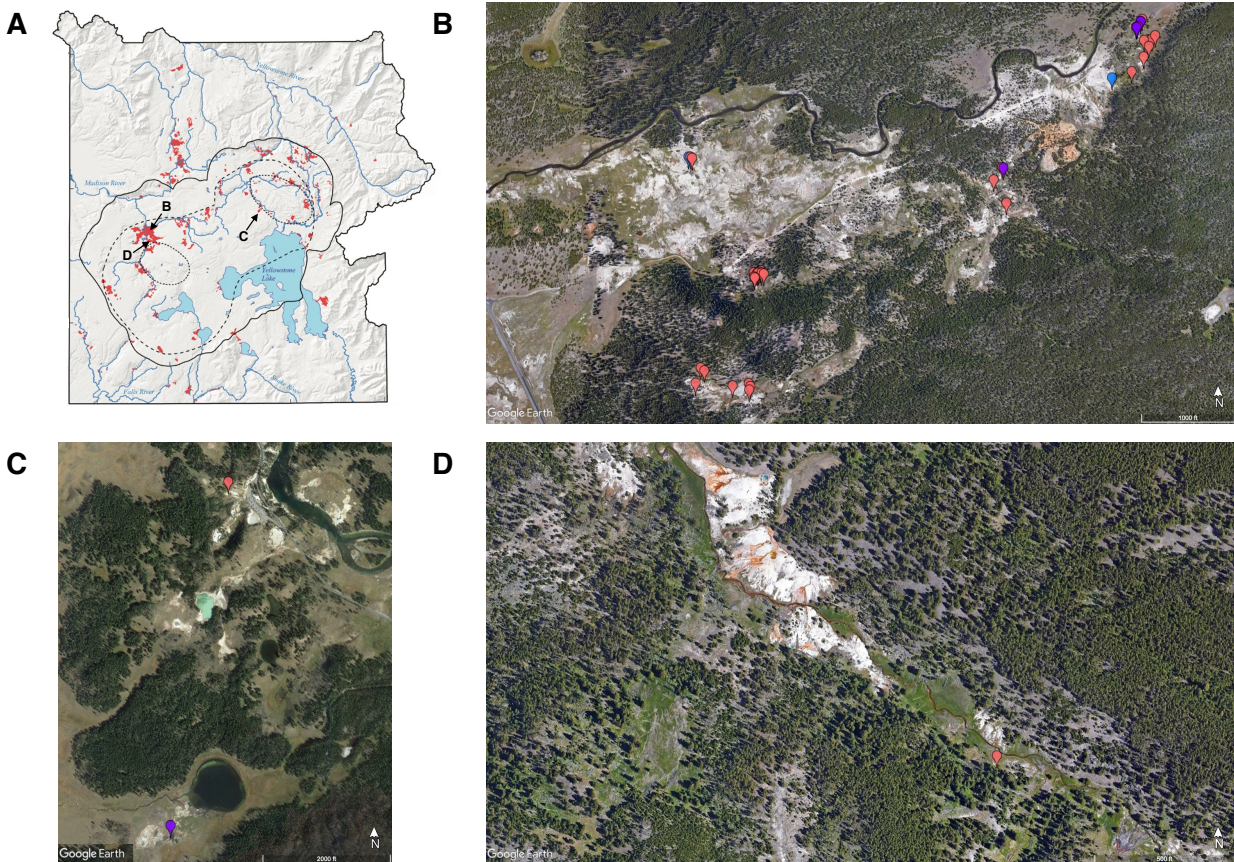


Fig. S5. Geographical distribution of geothermal features in Yellowstone National Park in which *Archaeoglobi*-related *mcrA* genes ($n = 36$) and *Ca. M. hypatiae*-related 16S rRNA genes ($n = 6$) were detected. Features are located in the (A) Map of Yellowstone National Park Wyoming, USA modified from Vaughan *et al.* 2014 (24) (B) Lower Culex Basin ($n = 36$), (C) Mud Volcano Region ($n = 2$), and (D) the White Creek Area ($n = 1$). These features spanned a wide pH (2.61-9.35) and temperature (18.4-93.8 °C) range. Features in which *mcrA* were detected are marked in red, while features with related 16S rRNA genes are shown in blue. Features in which both amplicons were detected are colored in purple. For details on these sites, their *mcrA* data, water geochemistry, and exact location, see Lynes & Krukenberg *et al.*, 2023. Image source: Google Earth.

Description of Available Supplementary Datasets

SI Dataset S1. Extended metagenome assembled genome (SIT-MG) and isolate genome statistics. Seqs, sequences; avg_cov, average coverage; avg_gc, average G+C content; % rel. abund., percent relative abundance.

SI Dataset S2. GCMS measurements of masses 16 (CH₄), 17 (¹³CH₄), and 19 (¹²CD₃H) during the isotope tracing experiment. Percent of labeled methane is calculated as a fraction of provided labeled substrate. Stdev, standard deviation.

SI Dataset S3. Gas chromatograph FID measurements of ¹²CH₄ during isotope tracing experiment. NA, not available/measured.

SI Dataset S4. Gas chromatograph FID measurements of CH₄ during temperature optimum experiment. NA, not available/measured.

SI Dataset S5. Inventory of genes expressed by *Ca. M. hypatiae* LCB24 under methanogenic conditions and as depicted in Fig. 5. Expression levels averaged across six replicates are reported in reads per kilobase of transcript per million mapped reads (RPKM).

References

1. S. Buessecker *et al.*, Mcr-dependent methanogenesis in Archaeoglobaceae enriched from a terrestrial hot spring. *The ISME Journal* 10.1038/s41396-023-01472-3 (2023).
2. M. M. Lynes *et al.*, Diversity and function of methyl-coenzyme M reductase-encoding archaea in Yellowstone hot springs revealed by metagenomics and mesocosm experiments. *ISME Communications* **3**, 22 (2023).
3. A. Apprill, S. McNally, R. Parsons, L. Weber, Minor revision to V4 region SSU rRNA 806R gene primer greatly increases detection of SAR11 bacterioplankton. *Aquatic microbial ecology : international journal* **75**, 129-137 (2015).
4. E. Bolyen *et al.*, Reproducible, interactive, scalable and extensible microbiome data science using QIIME 2. *Nature Biotechnology* **37**, 852-857 (2019).
5. M. Martin, Cutadapt removes adapter sequences from high-throughput sequencing reads. *2011* **17**, 3 (2011).
6. B. J. Callahan *et al.*, DADA2: High-resolution sample inference from Illumina amplicon data. *Nat Methods* **13**, 581-583 (2016).
7. C. Quast *et al.*, The SILVA ribosomal RNA gene database project: improved data processing and web-based tools. *Nucleic Acids Research* **41**, D590-D596 (2012).
8. N. M. Davis, D. M. Proctor, S. P. Holmes, D. A. Relman, B. J. Callahan, Simple statistical identification and removal of contaminant sequences in marker-gene and metagenomics data. *Microbiome* **6**, 226 (2018).
9. T. Aramaki *et al.*, KofamKOALA: KEGG Ortholog assignment based on profile HMM and adaptive score threshold. *Bioinformatics* **36**, 2251-2252 (2019).
10. S. Lu *et al.*, CDD/SPARCLE: the conserved domain database in 2020. *Nucleic Acids Res* **48**, D265-D268 (2020).
11. D. Sondergaard, C. N. Pedersen, C. Greening, HydDB: A web tool for hydrogenase classification and analysis. *Sci Rep* **6**, 34212 (2016).
12. M. Blum *et al.*, The InterPro protein families and domains database: 20 years on. *Nucleic Acids Research* **49**, D344-D354 (2020).
13. S. Neukirchen, F. L. Sousa, DiSCo: a sequence-based type-specific predictor of Dsr-dependent dissimilatory sulphur metabolism in microbial data. *Microb Genom* **7** (2021).
14. S. Neukirchen, F. L. Sousa, DiSCo: a sequence-based type-specific predictor of Dsr-dependent dissimilatory sulphur metabolism in microbial data. *Microbial Genomics* **7** (2021).
15. M. N. Price, P. S. Dehal, A. P. Arkin, FastTree 2--approximately maximum-likelihood trees for large alignments. *PLoS One* **5**, e9490 (2010).
16. R. C. Edgar, MUSCLE: multiple sequence alignment with high accuracy and high throughput. *Nucleic Acids Res* **32**, 1792-1797 (2004).
17. K. Katoh, D. M. Standley, MAFFT Multiple Sequence Alignment Software Version 7: Improvements in Performance and Usability. *Molecular Biology and Evolution* **30**, 772-780 (2013).
18. S. Capella-Gutiérrez, J. M. Silla-Martínez, T. Gabaldón, trimAl: a tool for automated alignment trimming in large-scale phylogenetic analyses. *Bioinformatics* **25**, 1972-1973 (2009).
19. B. Q. Minh *et al.*, IQ-TREE 2: New Models and Efficient Methods for Phylogenetic Inference in the Genomic Era. *Molecular Biology and Evolution* **37**, 1530-1534 (2020).

20. A. Rusch, J. P. Amend, Order-specific 16S rRNA-targeted oligonucleotide probes for (hyper) thermophilic archaea and bacteria. *Extremophiles* **8**, 357-366 (2004).
21. D. A. Stahl, Development and application of nucleic acid probes in bacterial systematics. *Nucleic Acid Techniques in Bacterial Systematics*, 205-248 (1991).
22. A. Pernthaler, J. Pernthaler, R. Amann, Fluorescence in situ hybridization and catalyzed reporter deposition for the identification of marine bacteria. *Applied and environmental microbiology* **68**, 3094-3101 (2002).
23. G. A. Schaible, A. J. Kohtz, J. Cliff, R. Hatzenpichler, Correlative SIP-FISH-Raman-SEM-NanoSIMS links identity, morphology, biochemistry, and physiology of environmental microbes. *ISME Communications* **2**, 52 (2022).
24. R. G. Vaughan, H. P. Heasler, C. Jaworowski, J. B. Lowenstern, L. P. Keszthelyi, *Provisional maps of thermal areas in Yellowstone National Park based on satellite thermal infrared imaging and field observations* (US Department of the Interior, US Geological Survey, 2014).